NTNU
Norwegian University of
Science and Technology

Evaluation of Acousto-Optic Tunable Filter for Wavelength Dependent Measurements of Waveguides

Vilde Aasvær Sømnes

Master of Science in Physics and Mathematics
Submission date: June 2017
Supervisor: Ursula Gibson, IFY

Norwegian University of Science and Technology
Department of Physics

Evaluation of Acousto-Optic Tunable Filter for Wavelength Dependent Measurements of Waveguides

Vilde Aasvær Sømnes

June 2017

MASTER'S THESIS

Department of Physics

Norwegian University of Science and Technology

Supervisor: Professor Ursula Gibson

Abstract

The main part of the work done for this master's thesis have been to implement and characterize a setup that would allow for wavelength dependent measurements of losses in waveguides. A plasma enhanced white light source have been used with an Acousto-Optic Tunable Filter (AOTF) to filter out a narrow bandwidth of wavelengths for wavelength dependent measurements.

The AOTF is designed to operate with a white light laser and the first part of the work was to determine the required characteristics of the input beam and to make the plasma enhanced white light source work with the AOTF. It was found that the light going into the Acoust-optic tunable filter had to be collimated, polarized and sent straight into the filter. Consequently, a setup was designed and implemented to satisfy these requirements.

Thin film waveguides were spin-coated to test the different source and detection schemes. This has not been a study of the losses in waveguides, but an investigation of what setup will allow for wavelength dependent measurements of losses in waveguides and what limitations the various setups have. The losses were found for different wavelengths in the range from 600 nm to 1100 nm to show the application of the setups that were designed, when using a Silicon or a Germanium detector in one setup configuration, and when using a spectrometer in a different setup.

Different detection schemes, including a microscope camera, a USB spectrometer, and a Germanium or Silicon detector with a lock-in detector and a scanning fiber probe were used. Measuring the losses with the spectrometer enabled measurements of all wavelengths at the same time, but the signal-to-noise ratio was fairly low and the scanning and data acquisition process was manual, and therefore time consuming and with a low resolution. The detection of the scattered light using a lock-in amplifier with a detector gave a higher signal-to-noise ratio which allowed for longer scans.

Sammendrag (Abstract in Norwegian)

Hoveddelen av arbeidet utført i forbindelse med denne masteroppgaven har vært å implementere og karakterisere et oppsett som kunne brukes til bølgelengdeavhengige målinger av tap i bølgeledere. En plasma forsterket hvittlys-kilde har blitt brukt sammen med et akusto-optisk justerbart filter for å filtrere ut en fraksjon av bølgelengdene i det hvite lyset. Dette har så blitt brukt i bølgelengdeavhengige målinger.

Det justerbare filteret er laget for å kunne brukes med en hvittlys laser og innledningsvis var det nødvendig å finne ut hvilke egenskaper lyset sendt inn til filteret måtte ha for at det skulle fungere optimalt. Det viste seg at lyset måtte være kollimert, polarisert og bli sendt rett inn i filteret. Et oppsett ble derfor utviklet og implementert for å oppfylle disse kravene.

Bølgeledere ble laget ved å spinn-belegge en tyn film på et substrat, som ble brukt til å teste de forskjellige kildene og oppsettene for deteksjon. Dette har ikke vært en studie av tapene i bølgeledere, men det er en undersøkelse av hvilket oppsett som muliggjør måliger av de bølgelengdeavhengige tapene i bølgeledere og hvilke begrensninger de forskjellige oppsettene har. Tapet ble funnet for flere bølgelengder mellom 600 nm og 1100 nm ved å bruke en Silisium- eller Germaniumdetektor i et oppsett, og ved å bruke et spektrometer i et annet oppsett.

Ulike konfigurasjoner for deteksjon, med et mikroskopkamera, et USB spektrometer og en germanium- eller silisiumdetektor med en innlåsningsforsterker (lock-in) og en fiber ble brukt. Ved å bruke et spektrometer for å måle tapet var det mulig å måle alle bølgelengdene samtidig, men forholdet mellom signal og støy er forholdsvis lavt og datainnsamlingen var manuell og derfor tidskrevende og med lav oppløsning. Detekteringen av det spredte lyset ved bruk av en innlåsningsforsterker og en detekor ga et høyere forhold mellom signal og støy som gjorde det mulig å ta målinger lengre ut i bølgelederen.

Preface

The work presented in this report has been a part of my Master's thesis in physics as part of the study program of Applied Physics and Mathematics at NTNU. The project has been carried out during the spring semester of 2017, and it has been a continuation of the work done for the specialization project carried out in the fall semester of 2016. It is assumed that the reader of this report has some basic knowledge in physics and optics.

Trondheim, 2017-06-25

Vilde Aasvær Sømnes

Acknowledgment

First, I would like to thank my supervisor, Professor Ursula J. Gibson. Her knowledge, know-how and great ideas have helped solve the various challenges that I was faced with while working on this thesis. Her enthusiasm and ability to find possible solutions are valuable skills that have been very helpful in the lab and truly inspirational.

I would also like to thank Ph.D. candidate Trygve Sørgård for all help in the lab, letting me borrow his equipment and for giving me valuable feedback on the thesis. The data acquisition process would have been extremely more time consuming without the automated setup with the stepper motor and I am grateful that I could borrow it.

A thank you goes to Ph.D. candidate Per Magnus Walmsness for letting me have access to the white light laser and borrowing it. I would also like to thank Department Engineer Vedran Furtula for helping me modulate the signal from the AOTF, enabling measurements using a lock-in amplifier. Professor Justin Wells and Professor Ulf Østerberg should also be thanked for their help when Ursula was away. Last, but not least, I would like to thank my brother for proofreading this thesis.

V.A.S

Acronyms

AOTF	Acousto-Optic Tunable Filter
FWHM	Full Width at Half Maximum
GUI	Graphical User Interface
IR	Infrared
LDLS	Laser Driven Light Source
NIR	Near-Infrared
PMMA	Polymethyl Methacrylate
PS	Polystyrene
RF	Radio Frequency
UV	Ultraviolet

Contents

Abstract i

Sammendrag ii

Preface iii

Acknowledgment iv

Acronyms v

1 Introduction **3**

2 Theory **5**

2.1 Acousto-Optic Tunable Filter 5

2.2 Planar Waveguides* 11

2.2.1 Calculating the Thickness of Thin Films 17

2.3 Coupling Techniques* 19

2.3.1 End-Fire Coupling* 19

2.4 Losses in Waveguides* 20

2.4.1 Loss Mechanisms 21

2.4.2 Measuring losses* 22

3 Method **23**

3.1 Sending Light Into the AOTF 23

3.1.1 AOTF input 24

3.1.2 AOTF Output and Throughput 28

3.2 Making Thin Film Waveguides 30

3.2.1 Spin Coating 30

3.2.2 Selection of Materials 31

3.3 Measuring Losses in Planar Waveguides 32

4 Results and Discussion **37**

4.1 Characterization of the Experimental Setup 37

4.1.1 Input to the AOTF 37

4.1.2 Output from AOTF 45

4.2 Thin Films 45

4.2.1 Agarose Film 46

4.2.2 Polymethyl Methacrylate Film 47

4.2.3 Polystyrene Film 48

4.3 Losses in Polystyrene Thin Film Waveguide 49

4.3.1 Laser Driven Light Source 49

4.3.2 White Light Laser and Spectrometer 51

4.3.3 White Light Laser and Lock-in Amplification 56

5 Conclusion and Further Work **65**

5.1 Experimental Setup 65

5.2 Loss measurements 65

5.3 Further work 66

A Detailed Description of the Experimental Setup **69**

A.1 Input to AOTF 69

A.2 Output from AOTF 70

B Calculations **71**

Bibliography **73**

Chapter 1

Introduction

Optical waveguides confines and lead light in the waveguide. For a waveguide to be useful, the attenuation of the waves traveling through it has to be low over a wide range of wavelengths. A way to measure the losses for various wavelengths can be to use different filters or lasers that emit at different wavelengths. An easy alternative is by using a tunable filter. An Acousto-Optic Tunable Filter (AOTF) is an electrically tunable filter which can been used in combination with a white light source to make a tunable light source for measurements of wavelength dependent losses in waveguides.

AOTFs are electronically tunable with a fast response. The AOTF contains a crystal that is excited with acoustic waves. As the acoustic waves propagate through the crystal, the variations in the density of the crystal causes changes in the refractive index of the crystal[1]. The changes in the refractive index acts as a diffraction grating for light sent in on the crystal where the wavelength of the diffracted light depends on the wavelength of the acoustic wave.

The AOTF used here is from Fianium and it is originally designed to operate with a white light laser, made by the same manufacturer. The focus of this thesis is to investigate if the AOTF can be used with a different light source that is not as powerful as the white light laser. This could lead to a setup that allows for measuring wavelength dependent losses in waveguides. A plasma enhanced white light source with a fiber coupled output has been the main alternative to the white light laser, but other light sources have also been investigated. Others have reported the use of an AOTF with a xenon arc lamp[2] where the output from the

filter has been coupled into a fiber bundle, in contrast to the setup presented here which is coupled into a single fiber. A different tunable light source with an integrated AOTF is available [3]. This tunable light source has an output power of 200 µW by using a 6.35 mm diameter core fiber.

Using a white light source that is less powerful and less hazardous than a white light laser enables the setup to be operated by less experienced personnel. The setup should allow for preliminary measurements of wavelength dependent measurements of losses in waveguides, before one can move on to using the more powerful setup with the white light laser for measurements that require higher accuracy. This setup can also be used for measuring the losses in different geometries, not just the two-dimensional geometry that is presented here, but also in semiconductor core fibers. The equipment is widely applicable, not only to loss measurements, but also to fluorescence and other optical properties of interest.

The waveguide that has been used to asses the performance of the setup has been a polystyrene thin film on a quartz substrate. The losses in the waveguide are measured by detecting the amount of light scattered out of the surface of the waveguide by scanning the surface of the waveguide with a pick-up fiber. This is a non-destructive method to find losses in waveguides which rely on the assumption that the light scattered out of the surface of the waveguide is proportional to the light propagating through the waveguide[4]. In waveguides with low losses, the fraction of light that is scattered out of the waveguide is small compared with the amount of light that is going through the waveguide. Thus, the throughput of the AOTF has to be as high as possible to get a detectable signal of the scattered light.

The approach to making the AOTF work with an alternative white light source than the white light laser is described in the following report as well as the production of different waveguides and measurements of losses in them.

Chapter 2

Theory

The following section will review the theory of Acousto-optic Tunable Filters, waveguides and the different techniques for coupling into a waveguide. Finally, the loss mechanisms in waveguides will be discussed. The parts on waveguides and coupling techniques are completely or partially taken from my specialization project, written last semester as a preparation for the master's thesis. These parts are marked with an asterisk (*).

2.1 Acousto-Optic Tunable Filter

An Acousto-Optic Tunable Filter contains an optical transparent crystal which is excited with acoustic waves. As the acoustic waves travel through the crystal, the refractive index change in response to the wave. This makes the crystal act as a diffraction grating for light that is incident on the crystal. AOTFs are used in many applications such as in tunable lasers [5], [6], and in optical reflectometry [7].

The main component in an AOTF is an optical transparent crystal which is connected to a piezoelectric crystal. The piezoelectric crystal is an electrical transducer and electrical radio frequency (RF) signals are converted to mechanical oscillations in it. The mechanical waves in the piezoelectric crystal set up acoustic waves in the optical transparent crystal which travel through the material and are absorbed at the other end. The acoustic waves cause the lattice structure to compress and relax in response to the oscillations of the acoustic waves. This leads to periodic variations of the refractive index in the crystal, resulting in a material

which will act as a diffraction grating for light incident on the crystal[8].

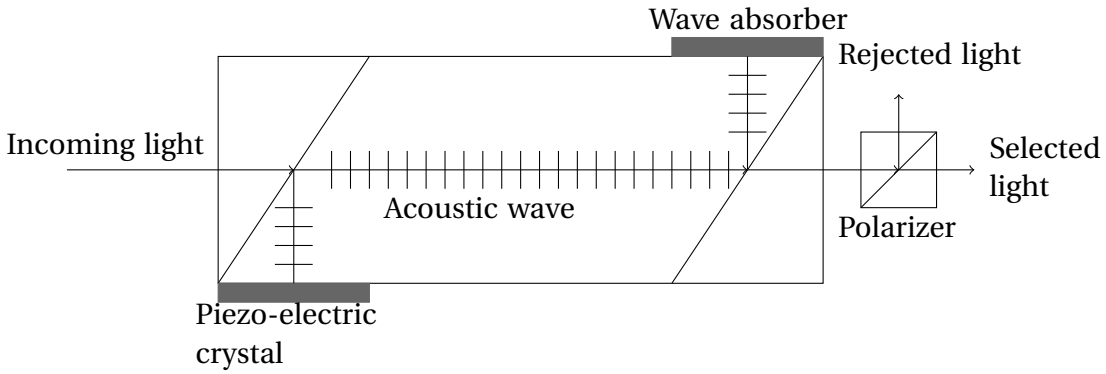

Figure 2.1: The acoustic wave travels through the crystal from the piezo-electric crystal to the acoustic wave absorber. The incoming light travels along the acoustic wave, and this is therefore a collinear AOTF. The light that interacts with the acoustic wave will change polarization. The portion of the light that has changed its polarization is let through a polarizer, while the rest is rejected. The figure is taken from [9].

There are two different configurations of AOTFs, one where the direction of the light is parallel with the direction of the acoustic wave as shown in fig. 2.1. This is called a collinear AOTF. Here, the polarization of the incoming light is changed when it is diffracted. Since the AOTF is collinear, the incoming and the diffracted light will travel in the same direction and a polarizer is used to only let through the light that is diffracted. The second type of AOTFs are the non-collinear, where the propagation direction of the light beam forms an angle with the propagation direction of the acoustic wave[10], as shown in fig. 2.2.

The incident light beam, with a momentum $\mathbf{p_i}$, will be diffracted when the following condition is met

$$\mathbf{p_d} = \mathbf{p_a} + \mathbf{p_i}$$

where $\mathbf{p_d}$ is the momentum of the diffracted light and $\mathbf{p_a}$ is the momentum of the acoustic wave[11]. This condition can be rewritten using the wave vectors of the acoustic wave, the incoming and diffracted light,

$$\mathbf{k_d} = \mathbf{k_a} + \mathbf{k_i}. \tag{2.1}$$

Following the treatment in [12], the momentum conservation in collinear AOTFs gives

$$\frac{n_d}{\lambda_0} = \frac{n_i}{\lambda_0} + \frac{f_a}{v_a}, \tag{2.2}$$

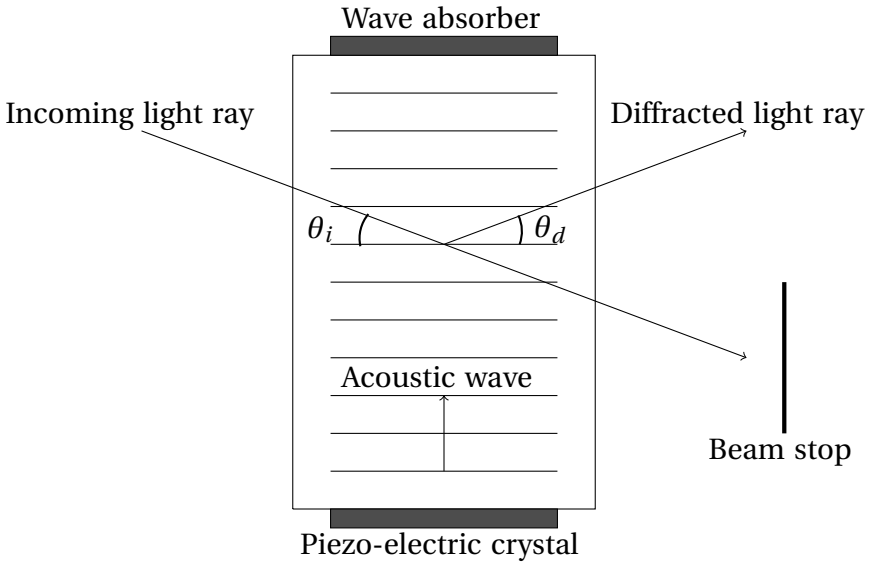

Figure 2.2: The setup of a non-collinear AOTF is shown. An acoustic wave travels through a optically transparent crystal which sets up a diffraction grating in the crystal which diffracts light going through the crystal. The figure is taken from [1].

where the relations

$$k_d = \frac{2\pi n_d}{\lambda_0},$$
$$k_i = \frac{2\pi n_i}{\lambda_0},$$
$$k_a = \frac{2\pi f_a}{v_a},$$

have been used. n_d and n_i are the refractive indices of the diffracted and incoming light, respectively, λ_0 is the wavelength of the diffracted light in vacuum, f_a is the frequency of the acoustic wave with a velocity v_a, and π has its usual mathematical value. Solving eq. (2.2) with respect to λ_0 gives

$$\lambda_0 = \frac{v_a \Delta n}{f_a}. \tag{2.3}$$

The birefringence, $\Delta n = n_d - n_i$, is introduced under the assumption that the polarization of the diffracted light is along the optic axis of the crystal and the polarization of the input light is perpendicular to the optic axis. From eq. (2.3) it is seen that the wavelength of the diffracted light depends on the frequency of the RF signal and the velocity of the acoustic wave in the crystal, as well as the birefringence.

The geometry in a non-collinear AOTF is different, which leads to a different treatment of the condition in eq. (2.1). In addition, there is a difference if the crystal in the AOTF is isotropic or anisotropic. Still following the development in [12], the isotropic case is explained first and then the anisotropic case. The AOTF used here is an anisotropic non-collinear AOTF.

The configuration in a non-collinear AOTF is shown in fig. 2.2 and θ_i is the angle of incidence. The diffraction is characterized as Bragg diffraction if the crystal is isotropic or if the diffraction process does not change the polarization of the light. In the direction normal to the acoustic wave vector, the condition in eq. (2.1) gives.

$$\begin{aligned} k_d \cos\theta_d &= k_i \cos\theta_i, \\ \frac{n_d}{\lambda_0} \cos\theta_d &= \frac{n_i}{\lambda_0} \cos\theta_i, \\ \theta_d &= \theta_i, \end{aligned}$$

where it has been used that $n_d = n_i = n$ in an isotropic medium. The condition eq. (2.1) in the direction of the acoustic wave vector gives

$$\begin{aligned} k_d \sin\theta_d &= -k_i \sin\theta_i + k_a, \\ \frac{n_d}{\lambda_0} \sin\theta_d &= -\frac{n_i}{\lambda_0} \sin\theta_i + \frac{f_a}{v_a}, \\ \frac{n}{\lambda_0} \sin\theta_d &= -\frac{n}{\lambda_0} \sin\theta_i + \frac{f_a}{v_a}, \\ \sin\theta_i &= \frac{f_a \lambda_0}{2 n v_a}. \end{aligned}$$

Here, it has also been used that the refractive indices of the incident and diffracted beam are the same and the minus sign in front of the wave vector for the incident light is given by the geometry in fig. 2.3a. The wavelength of the light that is diffracted by the diffraction grating set up in the crystal depend on the frequency of the acoustic wave, but also the incident angle of the light. The diffracted beam does not travel in the same direction as the non-diffracted beam and the non-diffracted beam is sent into a beam stop, as illustrated in fig. 2.2.

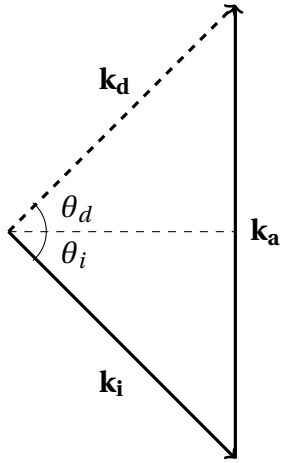

(a) The wave vecor diagram of and incoming light ray being diffracted in a isotropic medium.

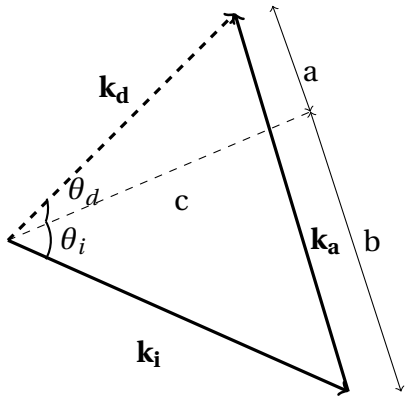

(b) The wave vector diagram of diffraction of light in an anisotropic mendium.

Figure 2.3: Vector diagrams of isotropic and anisotropic diffraction of light. The figures are taken from [12].

If the crystal is an anisotropic medium and the polarization of the diffracted light is changed, the interaction process between the light and the acoustic waves is different from previously described. To describe this, the geometry of the setup is the same as in fig. 2.2, but the input light is an extraordinary polarized wave. Both the input beam and the acoustic wave is moving perpendicular to the optic axis of the crystal. The diffraction process changes the polarization of the light from extraordinary to ordinary, meaning that the refractive index affecting the diffracted ray is n_o and the refractive index of the input beam is n_e, where $n_o \neq n_e$ since the crystal is anisotropic.

In the case of the anisotropic crystal, the angles θ_d and θ_i are not equal, as illustrated in fig. 2.3b, but can be found by solving eq. (2.1) and using the law of cosines which gives

$$k_a^2 = k_d^2 + k_i^2 - 2k_d k_i \cos(\theta_d + \theta_i).$$

This equation can be solved with respect to θ_d and θ_i and using the relations $a = k_d \sin\theta_d$, $b = k_i \sin\theta_i$, $c = k_i \cos\theta_i$ and $k_a = a + b$. After some rearranging of terms, the expressions

turn out to be

$$\sin\theta_d = \frac{\lambda_0}{2n_d\Lambda}\left[1 - \frac{\Lambda^2}{\lambda_0^2}(n_i^2 - n_d^2)\right], \tag{2.4}$$

$$\sin\theta_i = \frac{\lambda_0}{2n_i\Lambda}\left[1 + \frac{\Lambda^2}{\lambda_0^2}(n_i^2 - n_d^2)\right], \tag{2.5}$$

where the wavelength of the acoustic wave, $\Lambda = {}^{v}/_{f}$, has been introduced. The complete calculations to arrive at this result is given in appendix B.

In the collinear AOTF, it can be seen from eq. (2.3) that only light with the correct wavelength will be diffracted. The diffracted wavelength can be changed by changing the RF signal sent to the transducer, thus changing the frequency of the acoustic waves in the crystal. The interaction of the acoustic wave and the light occurs over the whole length of the crystal in the collinear AOTF, which leads to a narrow band width of the diffracted light[13].

From eqs. (2.4) and (2.5) it is evident that the wavelength that is diffracted also depends on the acoustic frequency, but here it is also dependent on the incident and diffracted angles as well as the refractive indices of the incident and diffracted beams.

The throughput of the AOTF has to be high for it to be useful. One of the parameters that influence the throughput is the diffraction efficiency, i.e the amount of light that is diffracted. It has been shown by Denes et al.[14] that the diffraction efficiency in AOTFs is dependent on the collimation of the input light, where a higher percentage of the input beam will be diffracted if it is well collimated than if it was poorly collimated. It has also been shown by J.E.B Oliveira[15] that the diffraction efficiency depends on the power of the acoustic wave and the phase mismatch between the light and the acoustic wave. The diffraction efficiency also depends on the interaction length, i.e. the length of the crystal in which the acousto-optic interaction occurs.

The interaction length between the acoustic wave and the light will influence the bandwidth of the diffracted light. A longer interaction length will result in a more narrow bandwidth, but it will also decrease the total optical output[16]. For measurements of the losses in

waveguides, a narrow band with of the filter is critical and a shorter length of the crystal can increase the throughput of the AOTF.

As illustrated by Katzka and Chang[17], both the collinear and the non-collinear AOTF configurations have many of the same traits. Both have high efficiency and high spectral resolution, to mention some, but the non-collinear configuration is easier to construct. The collinear design of an AOTF limits the selection of materials to only a few crystals and some of the most efficient acousto-optic crystals can not be used in a collinear AOTF[1]. Also, the filtered beam in a non-collinear AOTF is spatially separated from the incident light beam, which means that the filter can be constructed without polarizers.

2.2 Planar Waveguides*

A waveguide is a device that confines and guides waves. There are many kinds of waveguides, both ones that guides acoustic waves and others that guide electromagnetic waves. In this thesis, the waveguides that have been used have been waveguides that guide light in the visible and IR. This section will make clear what conditions that has to be fulfilled for the device to be able to guide waves and we will look at planar waveguides in particular.

The planar waveguide has parallel, planar boundaries in one direction (x), but the extension in the two other directions (y and z) are considered to be infinite compared to the extension in the x-direction, as illustrated in fig. 2.4. The extension of the waveguide in the x-direction is its thickness, d. All waveguides presented in this thesis have been thin films deposited on suitable substrates. The other surface of the thin film is in contact with air with a refractive index, n_a. The substrate has a refractive index, n_s, and the film has a refractive index, n. In an asymmetric waveguide, the refractive index of the substrate is not equal to the refractive index of air, which is the case in the waveguides presented here. The refraction of light at the film-air interface is shown in fig. 2.5a and Snell's law is given by

$$n_a \sin\theta_a = n \sin\theta_1.$$

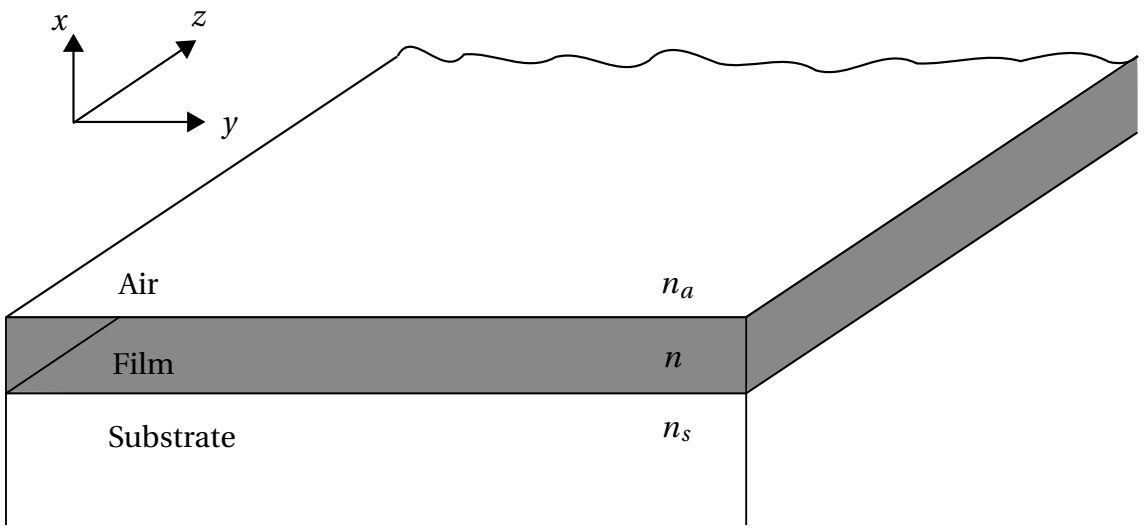

Figure 2.4: A planar waveguide with the extension in the y- and z-direction being much larger than the extension of the waveguide film in the x-direction. The waveguide film is on top of a substrate and is in contact with the air on its other surface. The figure is taken from [18].

The light in the waveguide has to be totally internally reflected for it to be guided in the waveguide, as illustrated in figure fig. 2.5b. Total internal reflection occurs when $\theta_a = 90°$, yielding

$$\sin\theta_1 = \frac{n_a}{n}.$$

With $\sin\theta_1 \leq 1$ always, we have that n_a must be smaller than n. The same condition is valid at the substrate-film interface and we have that

$$n \geq n_a, \tag{2.6}$$

$$n \geq n_s. \tag{2.7}$$

This shows that when making a thin film waveguide, the substrate has to be chosen based on its refractive index and the refractive index of the thin film material. The number of modes (discussed below) that can be supported in a waveguide, depends on the thickness of the film, the angular frequency of the wave, ω, and the refractive indices n, n_s and n_a.

Following the treatment in [18], we can look for solutions to Maxwell's wave equations for an electromagnetic wave in a waveguide. The wave equation for electromagnetic waves is

$$\nabla^2\mathbf{E}(\mathbf{r},t) = \frac{n^2(\mathbf{r})}{c^2}\frac{\partial^2\mathbf{E}(\mathbf{r},t)}{\partial t^2} \tag{2.8}$$

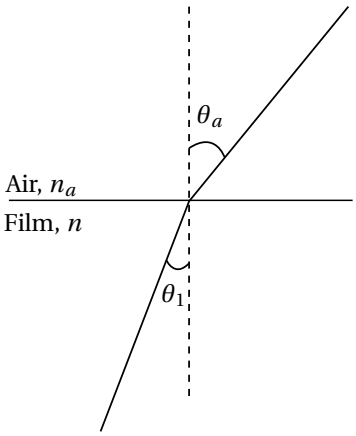

(a) Refraction of light rays at the interface of a waveguiding film with refractive index n and air with refractive index n_a.

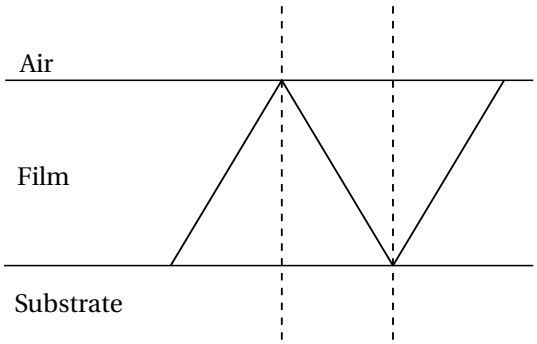

(b) Total internal reflection where the refractive index is larger than the refractive indices of the substrate and air.

Figure 2.5: Refraction of light at surfaces with different refractive indices.

where c is the speed of light in vacuum, $n(\mathbf{r})$ is the real part of the refractive index and $\mathbf{E}(\mathbf{r}, t)$ is the electric field at position $\mathbf{r}$ and time t. For monochromatic waves, one of the possible solutions is

$$\mathbf{E}(\mathbf{r}, t) = \mathbf{E}(\mathbf{r})\mathrm{e}^{i\omega t}$$

where $\omega = ck$ and k is the wave-number given by the wavelength of the monochromatic wave. By using the expression for ω, eq. (2.8) can be written

$$\nabla^2\mathbf{E}(\mathbf{r}, t) + k^2 n^2(\mathbf{r}) \cdot \mathbf{E}(\mathbf{r}) = 0. \tag{2.9}$$

Further, it is assumed that the wave is only propagating in one direction, e.g. the z-direction, and the electric field can then be expressed as

$$\mathbf{E}(\mathbf{r}) = \mathbf{E}(x, y)\mathrm{e}^{-i\beta z}$$

where β is the propagation constant. Plugging this expression into eq. (2.9) gives

$$\frac{\partial E(x,y)}{\partial x^2} + \frac{\partial E(x,y)}{\partial y^2} + \left(k^2 n^2(\mathbf{r}) - \beta^2\right)\mathbf{E}(x, y) = 0.$$

However, since the dimensions along the y-direction is much larger than in the x-direction, we may neglect the derivatives along the y-direction. For transverse electric (TE) waves, the

components E_x and E_z of $\mathbf{E}$ are zero and eq. (2.8) and its solution reduces to

$$\nabla^2 E_y = \frac{n^2}{c^2}\frac{\partial^2 E_y}{\partial t^2}$$

and

$$E_y(x,z,t) = \varepsilon_y(x)\mathrm{e}^{i(\omega t - \beta z)}. \tag{2.10}$$

$\varepsilon_y(x)$ depends only on x because the planar layers are assumed to be infinite in the y- and z-directions which excludes reflections and standing waves. The general solution for $\varepsilon_y(x)$ is

$$\varepsilon_y(x) = \begin{cases} A\mathrm{e}^{-qx} & \text{if } 0 \le x \le \infty \\ B\cos(hx) + C\sin(hx) & \text{if } -d \le x \le 0 \\ D\mathrm{e}^{p(x+d)} & \text{if } -\infty \le x \le -d \end{cases}$$

The coefficients A, B, C, D, q, h and p are constants that can be determined by the boundary conditions. The components of both the electric field and the magnetic field parallel to the surface must be continuous, i.e E_y, E_z, H_y and H_z must be continuous. From the Maxwell-Faraday equation in differential form, we have that $H_z \propto \frac{\partial E_y}{\partial x}$. Since H_z must be continuous, the derivative $\frac{\partial E_y}{\partial x}$ must also be continuous at the interfaces. These two conditions enable us to determine the constants A, B, C and D and $\varepsilon_y(x)$ is given by

$$\varepsilon_y(x) = \begin{cases} C'\mathrm{e}^{-qx} & \text{if } 0 \le x \le \infty \\ C'[\cos(hx) - \frac{q}{h}\sin(hx)] & \text{if } -d \le x \le 0 \\ C'[\cos(hd) + \frac{q}{h}\sin(hd)]\mathrm{e}^{p(x+d)} & \text{if } -\infty \le x \le -d \end{cases} \tag{2.11}$$

The constants q, h and p can be found by substituting eq. (2.11) into eq. (2.10) and using this expression in eq. (2.8). This yield

$$\begin{aligned} q &= \sqrt{\beta^2 - k^2 n_a^2} \\ h &= \sqrt{k^2 n^2 - \beta^2} \\ p &= \sqrt{\beta^2 - k^2 n_s^2} \end{aligned} \tag{2.12}$$

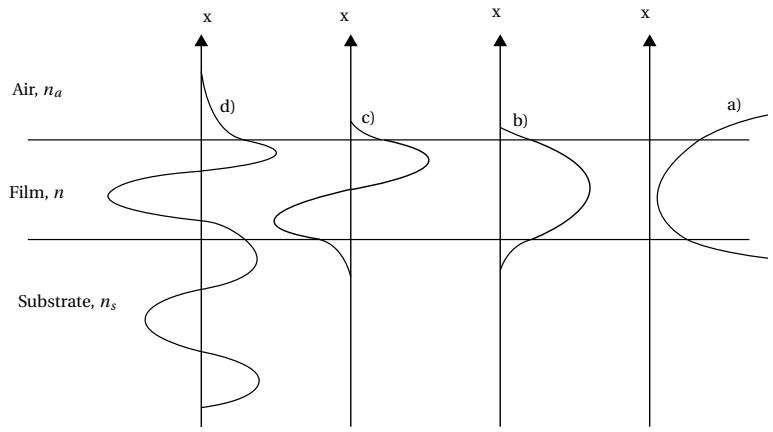

Figure 2.6: The figure shows some of the possible modes in a planar waveguide. The figure is taken from [18].

All the constants q, h and p are given by β which can be found by making $\frac{\partial E_y}{\partial x}$ continuous at $x = -d$. This gives, after some rearranging of the terms,

$$\tan(hd) = \frac{p+q}{h(1-pq/h^2)}. \tag{2.13}$$

This equation, with the conditions in eq. (2.12), gives a discrete set of allowed values for β. Each allowed value corresponds to an allowed mode. We see from the condition for h in eq. (2.12) that if $\beta > kn$, then the electric field is exponential in all three regions. This solution is non-physical because the exponential functions in the substrate and in the air, would be increasing, implying infinite energy. This mode and other possible modes are shown in fig. 2.6. Two of the possible modes for values of β between kn and kn_a are shown in b) and c). Here the wave is exponentially attenuated in the substrate and in the air and sinusoidal in the waveguide. Modes with β larger than kn_a, but less than kn_s is shown in d). The wave is attenuated in the air and has a form of a sine wave in the substrate. This kind of mode is possible, but it loses energy to the substrate and is attenuated over a short distance. It should be noted that the constant C' is arbitrary, but could be determined by normalization of $\varepsilon_y(x)$.

The cut-off condition for a waveguide is when the electric and magnetic fields becomes oscillatory in the substrate and the air. Then, the wave is no longer confined in the waveguide, but energy leaks into the air and the substrate. The cut-off occurs when the field spreads to

infinity in the substrate and we have that $\beta = kn_s$[19]. This gives

$$q = \sqrt{k^2 n_s^2 - k^2 n_a^2} = k\sqrt{n_s^2 - n_a^2}$$
$$h = \sqrt{k^2 n^2 - k^2 n_s^2} = k\sqrt{n^2 - n_s^2}$$
$$p = \sqrt{k^2 n_s^2 - k^2 n_s^2} = 0$$

Substituting this into eq. (2.13) then gives

$$\tan(hd) = \frac{q}{h}.$$

Solving for hd gives the solution

$$hd = m\pi + \arctan\sqrt{\frac{n_s^2 - n_a^2}{n^2 - n_s^2}}$$

where m is an integer and the term $m\pi$ is introduced due to the periodicity of the tangent-function. More specifically, m is the mode number and solving this equation with respect to m gives

$$m = \frac{2d}{\lambda}\sqrt{n^2 - n_s^2} - \frac{1}{\pi}\arctan\sqrt{\frac{n_s^2 - n_a^2}{n^2 - n_s^2}} \tag{2.14}$$

where k has been substituted according to the relation $k = \frac{2\pi}{\lambda}$. It is now possible to give an estimate of how many modes that can be supported in a particular waveguide with known refractive indices n, n_s and n_a and known thickness.

For transverse magnetic (TM) modes, with the field components H_y, E_x and E_z being non-zero, the calculations for the fields are similar to those of the TE-modes. This results in the field components

$$H_y(x,z,t) = \mathscr{H}_y(x)\mathrm{e}^{i(\omega t - \beta z)}$$
$$E_x(x,z,t) = \frac{i}{\omega\varepsilon}\frac{\partial H_y}{\partial z} = \frac{\beta}{\omega\varepsilon}\mathscr{H}_y(x)\mathrm{e}^{i(\omega t - \beta z)}$$
$$E_z(x,z,t) = -\frac{i}{\omega\varepsilon}\frac{\partial H_y}{\partial x}.$$

Similarly, to the transverse electric function, the transverse magnetic function can be expressed as

$$\mathscr{H}_y(x) = \begin{cases} -C'\frac{h}{\tilde{q}}\mathrm{e}^{-qx} & \text{if } 0 \le x \le \infty \\ C'[\frac{h}{\tilde{q}}\cos(hx) + \sin(hx)] & \text{if } -d \le x \le 0 \\ -C'[\frac{h}{\tilde{q}}\cos(hd) + \sin(hd)]\mathrm{e}^{p(x+d)} & \text{if } -\infty \le x \le -d \end{cases}$$

q, h and p are defined in eq. (2.12) and

$$\tilde{q} = \frac{n^2}{n_a^2}q.$$

The boundary conditions give the following constraint on allowed values for β

$$\tan(hd) = \frac{h(\tilde{p}+\tilde{q})}{h^2 - \tilde{p}\tilde{q}}$$

where $\tilde{p} = \frac{n^2}{n_a^2}p$.

2.2.1 Calculating the Thickness of Thin Films

For a thin film to be able to function as a waveguide, it has to support at least one mode. The number of modes depend on the thickness of the waveguide, as one can easily see from eq. (2.14). The thickness of a thin film can be found by examining the transmission spectra from a spectrophotometer, where interference fringes can be observed. In a spectrophotometer, light is sent in on the sample, as shown in fig. 2.7. At the first interface, some of the light will be reflected and the rest will be transmitted. The fraction of the incoming light that was transmitted will experience the same behavior at the second interface, where some of this light will be reflected back and some will be transmitted. The light that is reflected at the second interface will experience exactly the same as it hits the first interface again, where some of the light is transmitted and some is reflected. The light that is reflected will continue to move between the first and second interface until there is no light left. This will happen after only a few reflections if the transmission is high. The light transmitted the first

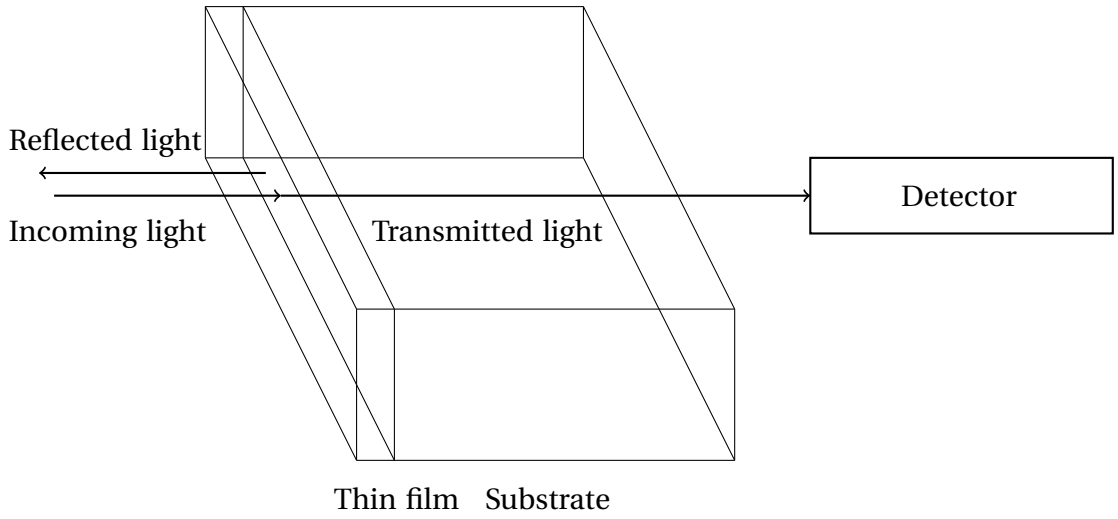

Figure 2.7: Light is sent in on a thin film on a substrate where some of the light is reflected at the first interface and some is transmitted. At the interface between the film and the substrate some of the light is transmitted and some is reflected back. A detector is placed at the back of the sample to collect the light that is transmitted.

time at the second interface will interfere with all the other light that was transmitted at the same interface, but after multiple reflections at the second and then the first interface. The light will experience a difference in path length which is equal to $2dn$, where n is the refractive index of the thin film and d its thickness. The light interferes constructively if the difference in path length is equal to an integer number of wavelengths and destructive interference occur when the path length is equal to half integer number of wavelengths [20], or

$$2dn = k\lambda \qquad \text{Constructive interference}$$
$$2dn = \left(k + \frac{1}{2}\right)\lambda \qquad \text{Destructive interference.}$$

where $k = 1, 2, 3, \ldots$ and λ is the wavelength of the light.

As stated by [20], the thickness of the film, d, is given by

$$d = \frac{1}{2\nu} \tag{2.15}$$

where

$$\nu = \frac{\frac{n(\lambda_1)}{\lambda_1} - \frac{n(\lambda_2)}{\lambda_2}}{N}.$$

N is the number of cycles between the peaks at λ_1 and λ_2. In order to know if a thin film will act as a waveguide, the thickness of the film has to be known. The method described here is an easy way to determine the thickness of a thin film.

2.3 Coupling Techniques*

To couple into a waveguide, the light should excite one or more of the modes supported by the waveguide. An easy and quick way to do this, is to send light in on the edge of the film. This method is called end-fire coupling and it excites all possible modes at once. There are several other methods of coupling into a planar waveguide, such as prism coupling and grating coupling, but these were not used here and are therefore not explained.

2.3.1 End-Fire Coupling*

The end-fire coupling technique is an easy way to couple guided modes into a waveguide. A light ray is directed at one of the edges of the waveguide and if the incident light contains one or more modes supported by the waveguide, the light is guided. The coupling efficiency should be as high as possible to send as much light as possible into the waveguides and there should be a good match between the mode profile in the waveguide and the modes contained in the light ray. Even though this is the easiest coupling technique, end-fire coupling into the waveguide will excite all the guided modes simultaneously and, in practice, it is not possible to excite one single mode.

Light is sent from a fiber with an exit angle of approximately 24°. The waveguide used here is a thin film with a thickness of approximately 0.4 µm. If we approximate the distance between the end of the fiber and the edge of the film to be $l = 5\,\mu\text{m}$, we can find the maximal coupling efficiency based on the geometry of the system as illustrated in figure fig. 2.8. The distance, l, is estimated based on pictures from the lab, where it is seen that the maximal distance is approximately 5 µm. From fig. 2.8, the radius, r_1, is given by

$$r_1 = l \tan \alpha$$

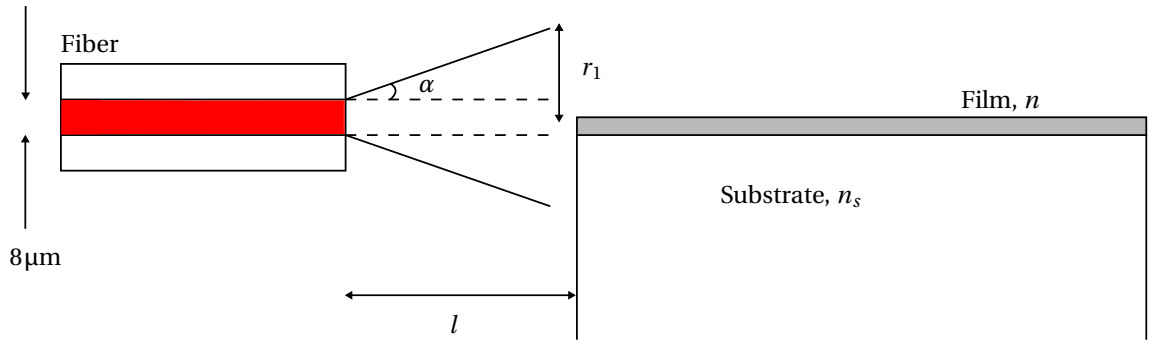

Figure 2.8: The set up of the end-coupling into the waveguide. The core of the fiber is 8µm and the exit angle of the light is $\alpha = 24°$. The area of the film which is illuminated can be approximated as a thin slab with height equal to the thickness of the film and a length equal to the diameter of the light cone at the edge of the film.

where α is the exit angle from the fiber. The film has a thickness d and the area of the film which is illuminated by the laser can be approximated with a rectangle with height equal to d and a length equal to $2r_1$. Thus, the area of the illuminated part of the film is given by

$$A_f = 2r_1 d.$$

The area of the light cone at the edge of the film is $A_l = \pi r_1^2$ and the percentage of light sent out from the fiber that actually hits the film is

$$\begin{aligned} \frac{A_f}{A_l} &= \frac{2r_1 d}{\pi r_1^2} \\ &= \frac{2 \cdot d}{\pi \cdot l \tan \alpha} \\ &\approx 11\% \end{aligned}$$

This means that more than 89% of the light is lost due to the geometry of the setup. In addition, there is mode mismatch and scattering at the surface of the film which will increase the losses further.

2.4 Losses in Waveguides*

As a mode travels through a waveguide, it is attenuated, and an important feature of a waveguide is its losses. The losses are measured by comparing the intensity of the light at a position, x, with the intensity of the light sent into the waveguide. The intensity of the light

is assumed to follow an exponential decline[21], which is given by

$$I(x) = I_0 \mathrm{e}^{-\alpha x} \tag{2.16}$$

where I_0 is the intensity of the light sent into the waveguide, α is the attenuation coefficient and $I(x)$ is the intensity at position x from the point at which the light enters the waveguide. The loss is usually stated in decibel per length unit, where the loss in decibel (dB) is given by

$$L_{dB} = 10\log_{10}\Big(\frac{I(x)}{I_0}\Big).$$

Using the expression in eq. (2.16) gives

$$\begin{aligned} L_{dB/cm} &= -10\alpha\log_{10}(\mathrm{e}) \\ L_{dB/cm} &\approx -4.34\alpha. \end{aligned} \tag{2.17}$$

2.4.1 Loss Mechanisms

There are several mechanisms that contribute to the losses in waveguides. One of the most dominant loss mechanism is scattering loss, caused by imperfections in the waveguide and at the interface between the substrate and waveguide. The imperfections can be contamination, porosity, grain boundaries and cracks. The guided light is diffused by the imperfections and the light is radiated out of the waveguide. If the impurities are smaller than the wavelength of the light guided in the film, Rayleigh's law states that the loss is proportional to $^1/_{\lambda^4}$ [22].

Other loss mechanisms are radiation losses and absorption losses. Light is radiated out of the waveguide when the refractive index of the waveguide is close to the refractive index of the substrate and the electromagnetic field leaks into the substrate. The radiation losses are only dominant in waveguides when the refractive indices of the waveguide and the substrate are similar. The refractive index of both the waveguide and the substrate vary with wavelength, thus the radiation loss will be a function of wavelength. To ensure the waveguide is able to guide over a wide range of wavelengths, the refractive indices of the substrate

and the film must satisfy the conditions in eqs. (2.6) and (2.7) over the same range of wavelengths.

Absorption loss occur when photons are absorbed as they are traveling through the waveguide. The photons can be absorbed by phonons in the waveguide, leading to a loss in optical power to thermal heat in the material. Photons can also be absorbed by exciting electrons to higher energy levels or be absorbed by impurities in the waveguide.

2.4.2 Measuring losses*

There are several methods of measuring the losses in waveguides. Some of these are the cutback method and the sliding prism method. The cutback method is a destructive procedure and the sliding prism method suffers from uncertainties due to the mechanical movement of the prisms[23]. The method for measuring the losses in a waveguide used here has been non-destructive where the light scattered out of the waveguide is detected along the streak of the guided light. This method relies on the assumption that the light scattered out of the waveguide is proportional to the light propagating through the waveguide and it is limited to waveguides where the losses are high enough that the light scattered out is detectable. This method will be explained in further detail in section 3.3.

Chapter 3

Method

The complete experimental setup is explained in detail in this section. The main components of the setup are the white light source, the filter and a detector. The filter is the AOTF, while different light sources have been used as well as different detectors. The approach to finding the required characteristics of the input beam is explained and an explanation of the setup is given. Further, the making of thin film waveguides are explained as well as the method of finding the losses in waveguides by detecting the light scattered out of them. The reason for making the waveguides was to have some waveguides for characterizing the experimental setup.

3.1 Sending Light Into the AOTF

The AOTF used in this thesis has been a Fianium AOTF-DUAL system which has two (NIR1 and NIR2) crystals in it. This gives it a tuning range from 650 nm to 2000 nm. Operating and choosing which wavelengths to filter through the AOTF is made easy by a graphical user interface (GUI) from the manufacturer. Both crystals are powered by a radio frequency driver and each driver has eight different channels, meaning that eight different wavelengths can be let through at once for each crystal. The AOTF-DUAL system can therefore let through sixteen different wavelengths at the same time. The AOTF should block all light except for the wavelengths that are chosen by the operator and it should block all wavelengths when no wavelengths are chosen.

Originally, the AOTF comes with a white light laser source which can be connected to the AOTF via an optical fiber. The fiber from the white light laser has an end piece that fits into the front piece of the AOTF, see fig. 3.1, ensuring the light enters the AOTF in the right way. It was not known what the "right way" was, and a major part of the work has been to figure this out. The white light laser and the AOTF are made to go together and designed to enable fast and easy coupling between the two. The white light source used instead of the white light laser has been a plasma enhanced white light source. The light source is a EQ99X Laser Driven Light Source (LDLS) from Energetiq and according to the specifications of the light source, it emits in the range from 190 nm to 2100 nm. The output from the LDLS is coupled into a multi-mode fiber.

3.1.1 AOTF input

There is very little information from the manufacturer of what the characteristics of the input light should be. A first step to making the AOTF function with other light sources was to assume beam characteristics based on the knowledge of the general design of AOTFs. The assumptions were that the light beam should be

- Sent straight into the AOTF
- Collimated
- The appropriate size
- Polarized

The first assumption is made based on the design of the input piece of the AOTF. The function of this piece is obviously to hold the end of the fiber going from the white light laser, but the construction of it suggests that it is crucial that the light is sent into the AOTF with the correct angle. The second assumption is made based on the assumed geometry in the AOTF. It is unknown if there are any optics before the light beam hit the crystal. If there are optics before the light hit the crystal, it most likely behaves best with a collimated beam that has the correct incoming angle. It may be possible to make the AOTF work with a beam that is not collimated, but then only a small fraction of the light will have the correct direction and a lot of the incoming light will be lost. The size of the crystal is not known, but if the beam is bigger than the crystal a lot of light will be lost there as well. Clearly, the beam should not

be bigger than the entrance aperture of the AOTF. The input piece of the AOTF also ensures the orientation of the beam being the same, thus ensuring the input light has the same polarization every time. This suggested that the light going into the AOTF had to be polarized.

When a collimated laser beam was sent into the AOTF at an angle, it was found that light would go through even when the AOTF was turned off or all the channels were closed. The AOTF itself is an enclosed box[1] and it is not known what is inside it except the crystals. It is therefore not obvious what causes the light to go through the AOTF when there is no RF signal sent to the crystal and the light is entering it on an angle. A possible explanation is that the light would not hit the crystal, but reflect on the walls inside the box, leading some of light to be scattered out of the AOTF. To ensure the light was not going into the AOTF on an angle, an alignment tool was designed by utilizing the front piece of the AOTF. The front piece, shown in fig. 3.1, is a hollow cylinder and the alignment tool was made to fit on the outside of this.

In addition, the light beam also has to be well collimated for it to only hit the crystal inside the AOTF and avoid some of the light being scattered out. The output fiber going from the white light source was therefore connected to a reflective collimator. The reflective collimator works over a broad band of wavelengths, unlike lenses which suffer from aberrations. The specific collimator used in this setup is a Thorlabs RC02SMA-F01 collimator which, according to the specifications, works best for single-mode fibers[24]. The fiber connecting the white light source with the reflective collimator is a multi-mode fiber, resulting in a non-collimated beam with a bigger beam diameter than expected from the specifications of the reflective collimator. For the experimental setup to work over a large range of wavelengths, the fiber connecting the LDLS to the collimator had to be multi-mode.

The UV-light from the plasma source is outside the operating wavelength range of the AOTF and the UV-light is filtered out due to safety reasons. The output of the reflective collimator goes into a lens tube containing a UV-filter from Thorlabs (FEL0500) with a cut-on frequency at 500 nm. Because the light is not perfectly collimated, a lens is placed after the UV-filter

[1] The warranty of the AOTF will be invalid if the box is opened.

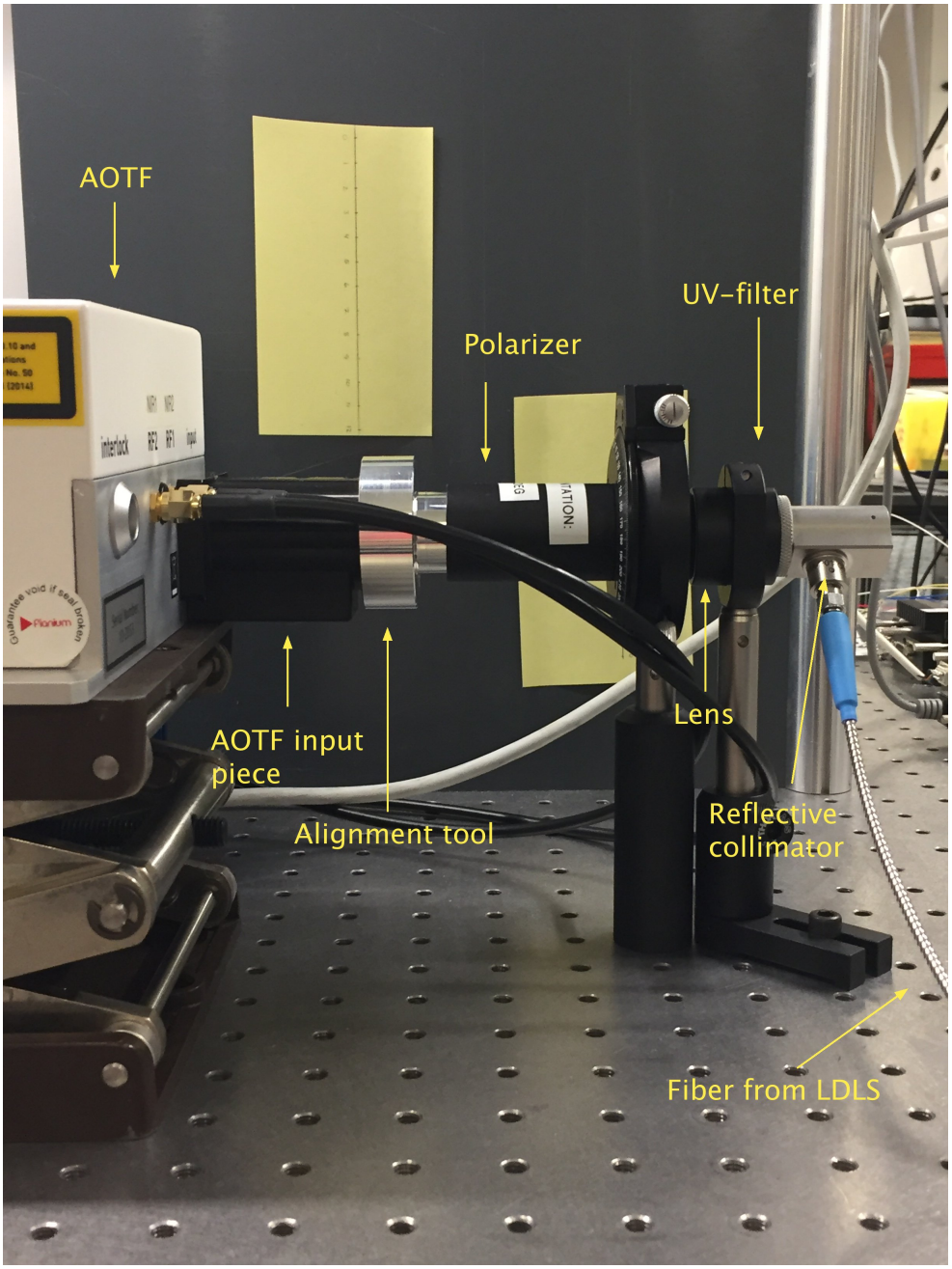

Figure 3.1: The image shows the components needed for sending light into the AOTF. The input fiber from the LDLS goes into the reflective collimator. This is attached to a lens tube which holds a UV-filer and a lens. The end of the lens tube goes to the end of a second lens tube containing the polarizer. The big wheel between the two lens tubes is there in order to rotate the lens tube containing the polarizer. The alignment tool fits into the end of the lens tube with the polarizer and it fits on the outside of the input piece of the AOTF, ensuring that the light beam goes straight into the AOTF.

in the lens tube to decrease the divergence angle. Even though the light is not perfectly collimated, it was found that the degree of collimation was good enough and that the AOTF blocks the light when no RF signal is applied to the crystal and the correct wavelength is let through when it is supposed to. It is not optimal that the beam is not collimated because

that means that some of the light is lost.

It was found that the light should be polarized before entering the AOTF. Even though the diffraction grating set up by the acoustic wave in the crystal acts as a polarizer, it was seen that to polarize the light before sending it into the AOTF was beneficial. When the light was un-polarized when entering the AOTF, a portion of the light that should be blocked by the AOTF, went out. A double Glan-Taylor polarizer from Thorlabs (DGL10) was placed inside a lens tube which was mounted on a PRM1 rotational mount, also from Thorlabs. The rotation mount enabled rotation of the plane of polarization, thus optimizing the input beam. The alignment tool, mentioned earlier, was made to fit on the outside of the front piece of the AOTF and on the inside of the lens tube containing the Glan-Taylor polarizer. This makes one long tube where the light goes through the polarizer, then through the alignment tool which is aligned with the lens tube holding the polarizer, and then through the front piece of the AOTF which is parallel with the alignment tool. The alignment tool was made so that it fits well into both the lens tube and the front piece of the AOTF with little room to move.

The lens tube containing the UV-filter and the lens, which the reflective collimator is attached to, cannot be attached to the lens tube holding the polarizer. This is because of the design of the rotational mount holding the lens tube with the polarizer. The rotation mount has a cylindrical hole going through it with hinges going almost all the way through. The lens tube holding the polarizer was therefore screwed into the rotation mount on one side. The UV-filter and the lens could be mounted in the same lens tube as the polarizer, but it is not possible to mount the reflective collimator on the rotation mount. Due to safety reasons, the reflective collimator was attached to a separate lens tube containing the UV-filter. The lens collimating the light from the reflective collimator was also mounted in the lens tube with the UV-filter, and the lens tube is placed close to the rotation mount to align the two as best as possible.

3.1.2 AOTF Output and Throughput

A tunable light source can be used for measuring wavelength dependent losses in waveguides or any other application where it is necessary to have a tunable light source. For it to have any practical use, the intensity of the light has to be high enough for it to be detected. It was therefore necessary to optimize how the output from the AOTF was picked up. The throughput of the AOTF should also be optimized to maximize the intensity of light that can be used for measurements.

The AOTF comes with a collimator that collimates its output and gathers the light into a fiber, as shown in fig. 3.2. The collimator fits into the output piece that is attached to the AOTF and its position can be changed by adjusting set screws that are located on the output piece. First, the light from the AOTF was coupled into the fiber that came with it using the collimator. The fiber was then coupled into a different fiber which had been stripped of its cladding and plastic cover and then cleaved. A fiber coupler from Thorlabs (ADAFCB1) was used to couple the two fibers. Some of the light is lost in the coupling between the two fibers and in an attempt to decrease the losses associated with coupling, the fibers were bare ferrule-coupled, meaning that the bare ferrules of the fibers are held together by a ceramic tube that goes on the outside of both ferrules.

The ferrule of the fiber going from the collimator can also be used directly to couple into the waveguide. The fiber has a core diameter of 62.5 µm and a numerical aperture of 0.275. The ferrule was mounted on a holder to couple into the waveguide with it. In an attempt to improve the amount of light going into the waveguide, a funnel collimator was used to collect the light at the output of the AOTF instead of the collimator that came with the AOTF. This was done because the funnel collimator could collect more light, but it does not fit into the output piece on the AOTF. The funnel collimator was therefore placed on a stand at the end of the output piece where it collected the light. The funnel collimator was connected to a fiber (Ocean Optics, P400-2UV/VIS) with a core diameter of 400 µm. Since the Ocean Optics fiber has a larger core diameter than the Thorlabs fiber, it is possible to direct more light into the fiber.

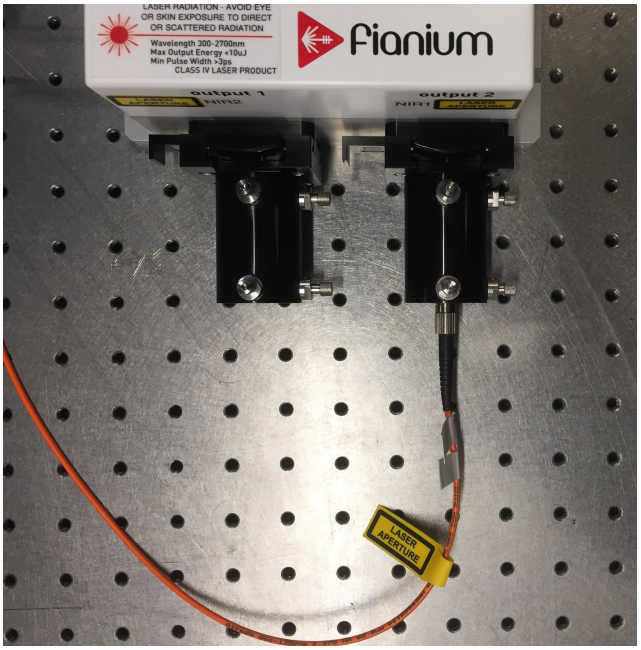

Figure 3.2: An image of the output pieces of the AOTF for the NIR1 and NIR2 outputs. A collimator is mounted inside the output piece of the NIR1 output and a fiber is attached to the collimator. This fiber is connected to a bare end fiber or used to couple directly into the waveguide using the bare end ferrule.

3.2 Making Thin Film Waveguides

The thin film waveguides made as a part of this thesis were made by spin coating and this process is described in the following section. Films of three different materials were made.

3.2.1 Spin Coating

Spin coating is a fast and easy way to deposit thin films on a substrate. A substrate is placed on a stand which is able to rotate. The substrate is held in place by a vacuum as the stand rotates. A solution with the desired film material is deposited on the substrate and the substrate accelerates to a high rotation speed. As the substrate with the solution rotates, the solution moves radially outwards due to the centrifugal force and the solution is spread out on the substrate, as illustrated in fig. 3.3. The rotation speed is then increased to eject the excess solution off the substrate, but the initial amount of solution that is placed on the substrate is not believed to influence the thickness[25]. The rotation speeds are programmed in the spin coater beforehand and the transition from one rotation speed to another happens automatically. As the substrate rotates, the solvent evaporates, leaving a film on the substrate. It was found that it was beneficial to have an initial rotation speed which was low to spread the solution and then increase the speed rapidly to eject most of the solution off the substrate, leaving just a thin film.

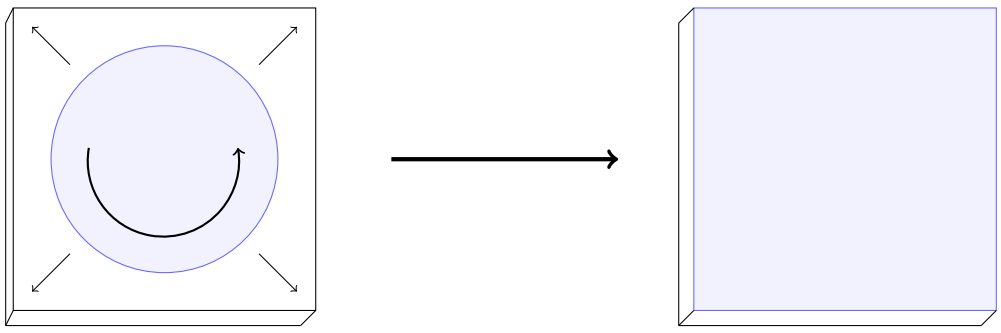

Figure 3.3: The thin film material in a solution (here illustrated in blue) is deposited on the substrate. As the substrate is rotated, the solution will be distributed over the surface of the substrate by the centrifugal force. The substrate will be completely covered in the film material, and when the solvent is evaporated, a thin film is left on the substrate.

3.2.2 Selection of Materials

A waveguide was needed to have a sample that could be used for looking at the wavelength dependent losses as a proof of principle for the setup that was made. The waveguide material had to have low enough losses for it to work as a waveguide, but not too low losses which would lead to the scattering being too low to be detected. The choice of waveguide material had to have a refractive index that was higher than the refractive indices of the chosen substrate and air. The three different materials all fulfilled these demands and they were readily available in the lab.

A solution of Agarose was made by dissolving Agarose powder in water, with a concentration of approximately $0.015\,\mathrm{g\,mL^{-1}}$. This particular concentration was selected based on the concentration used by Lee et al.[26]. The Agarose in water was heated in a microwave oven in order to dissolve the Agarose in the water. The viscosity of the Agarose solution depends on the temperature of the solution, and the viscosity of the solution seemed to influence the thickness of the film that was made. In addition to the viscosity of the solution, the rotation speed and the temperature of the substrate also influence the thickness of the film. The substrate was heated on a hot plate before it was transferred to the spin coater, but this transportation cooled down the substrate. Even though the Agarose solution was heated, the solution was deposited on the substrate by using a plastic pipette which was not heated. Not only was it necessary to control three parameters, but the transportation of the solution and the substrate made it difficult to control the temperatures. Many different combinations of temperatures of solution and substrate was combined with different rotation speeds, but without success in making any films that had the proper thickness to act as a waveguide. A sensible step was to change to a different material where the temperature would not affect the viscosity of the solution.

Polymethyl Methacrylate (PMMA) is a polymer and it is used for many different applications, such as thin films. The NanoLab at NTNU have written recipes on how to spin coat substrates with films of the desired thickness. The thickness needed for the film was calculated by choosing a suitable number of modes and then solving eq. (2.14) with respect to d.

The thickness needed to be approximately 2000 nm for the waveguide to be able to support at least one mode and an already prepared PMMA solution was chosen accordingly. First, the substrate was heated at a hot plate for approximately one minute at 180 °C. The solution was deposited on a quartz substrate and the spin coater was set to first rotate at 500 rpm for 5 s to spread the solution on the substrate. The rotation speed was then increased to 1500 rpm and held there for 45 s. The film was then left to dry completely for approximately 12 h.

Polystyrene (PS), also a polymer, was also used for making thin films. The PS solution was made by taking a couple of pieces of a polystyrene plastic container, approximately 0.2 g, and dissolve it in approximately 5 mL of toluene. The solution was placed on a quartz substrate and rotated, first at a speed of 2000 rpm for 2 s to spread the solution. The rotation speed was then increased to 4000 rpm for 180 s to make the film thinner and allow the toluene to evaporate. The films were then left overnight to let the toluene evaporate completely. Unlike the PMMA film, there was no recipe for making the film of the desired thickness and it was necessary to try different rotation speeds and rotation times to arrive at the procedure that made films with the correct thickness. The approach explained here is the method used for making the waveguide that was used in the loss measurements.

The thickness of all the films were found by spectrophotometry and calculated using eq. (2.15). The thin films that were polished to make a clean edge suitable for end-fire coupling.

3.3 Measuring Losses in Planar Waveguides

The losses in the waveguide was found by scanning the surface of the waveguide with a pick-up fiber that detected the amount of light scattered out of the waveguide. Under the assumption that the light scattered out of the waveguide is proportional to the light in the waveguide, the loss in the waveguide can be found. The light was end-fire coupled into the waveguide, where all the possible modes were excited.

To end-fire couple light into the waveguide, two different approaches were used. The bare

end of a ferrule or a drawn fiber was placed close to the edge of the waveguide and light was coupled into it. A drawn fiber was made by taking a fiber with a core diameter of 200 µm and removing the plastic coating. The fiber was then heated and drawn by pulling both ends of the fiber apart. The drawing process makes the diameter of both the core and cladding thinner, leaving a smaller core diameter. This makes it possible to couple into the waveguide more efficiently due to the core of the fiber being smaller and more similar in size to the thickness of the thin film waveguide, but the other end of the fiber is still thick and more light can be sent into the fiber.

The waveguide was coupled into by placing the fiber close to the polished edge of the waveguide and adjusting the height of the fiber to align it with the thin film. In order to see if light was coupled into the waveguide, the fiber and the waveguide was placed to form an angle smaller than 90° between the end of the fiber and the waveguide. When the light is coupled into the waveguide, the light refracts and the light will change direction. When the light goes straight ahead, the light goes over the waveguide, but when the light goes on an angle, the light is coupled into the thin film. A USB microscope camera was placed over the surface of the waveguide in order to observe this behavior. An image of the camera over the waveguide and the fiber is shown in fig. 3.4.

To measure the light scattered out of the waveguide, the surface of the waveguide was scanned with a pick-up fiber. The fiber was either connected to a spectrometer or a detector (Silicon or Germanium), but the setup was similar. The pick-up fiber could move in the x- and y-direction over the surface of the waveguide, detecting the light scattered out of the waveguide, as shown in fig. 3.5. When using the Spectrometer, the pick-up fiber was mounted on a stand that was moved manually by turning a micrometer screw for each direction, and the resolution of the micrometer screws are 10 µm. For each position at the surface of the waveguide, a spectrum of the light was detected and saved in a file. Using the spectrometer allows for detection of all eight wavelengths let through the AOTF at once and only one scan is necessary to get the wavelength dependent measurements of the losses in the waveguide. The number of counts for each wavelength in the spectrum is proportional to the intensity of the light at that wavelength and for each peak in the spectrum, the number of counts

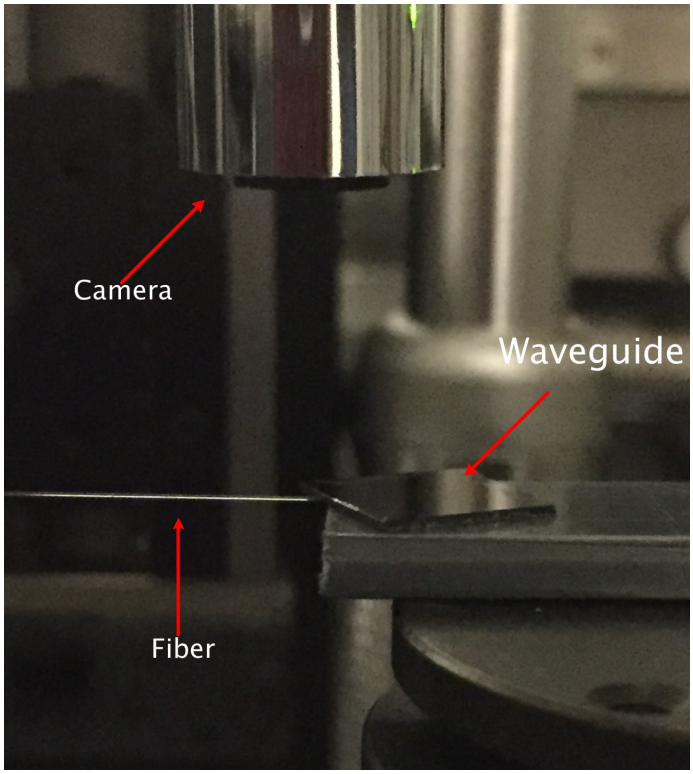

Figure 3.4: The setup for seeing when light is coupled into the waveguide. The fiber end is seen by the camera as well as the surface of the waveguide. When light is guided in the waveguide, there will be a visible streak of light being scattered out of the waveguide. This image is taken from the specialization project performed the fall semester of 2016.

were integrated. For each wavelength, the integrated number of counts at every point was plotted in a surface plot and the maximum of the integrated number of counts was found for each line along a constant y. The maximums and its corresponding position can then be used to find the intensity as a function of distance, which can be used to find the losses in the waveguide as explained in section 2.4.

A similar configuration was used when detecting the scattered light from the surface using the detector with a lock-in amplifier, but here the fiber was mounted on a stand that was connected to a stepper motor. The data acquisition was automatic, which means that the scan of the surface was automated. The detector was used with a lock-in, which makes the signal-to-noise ratio small even for low intensities of scattered light. However, when using the Silicon detector, one scan had to be performed for each wavelength.

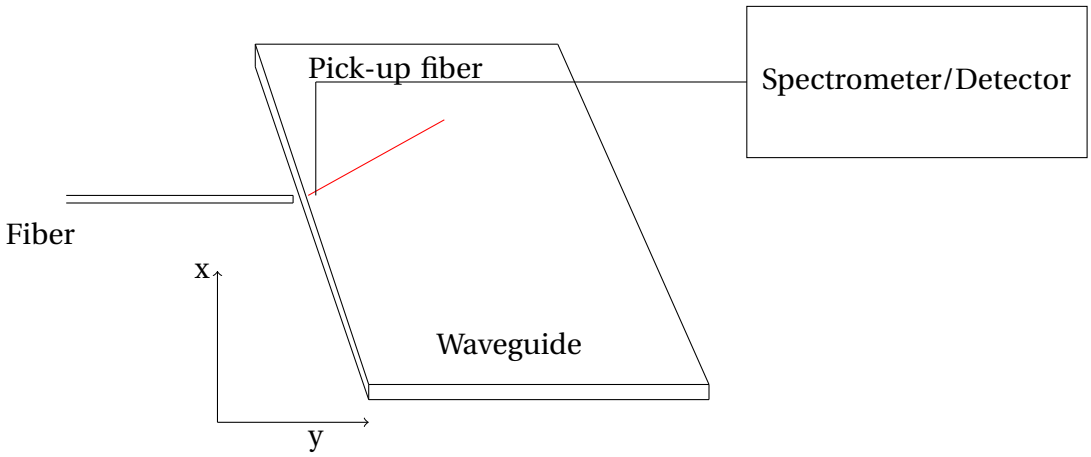

Figure 3.5: The experimental setup for detecting the light scattered out of the surface of the waveguide. The light is coupled into the waveguide by placing the fiber close to the edge of the waveguide. The detector moves over the surface of the waveguide in the x- and y-direction, giving a profile of the intensity distribution of the light scattered out from the surface of the waveguide.

Chapter 4

Results and Discussion

This section will first present the characteristics of the experimental setup made for this thesis and discuss what can be done to improve it. In following, the measurement of the thickness of the thin film waveguide is presented and finally, the application of the setup by measuring the wavelength dependent losses in the PS waveguide are presented.

4.1 Characterization of the Experimental Setup

Due to the process of designing a setup that can be used as a tunable light source is a considerable part of this thesis, the characterization of the system is crucial and it is presented and discussed in this section.

4.1.1 Input to the AOTF

The plasma enhanced white light source is said by the manufacturer to be emitting in the range from 190 nm to 2100 nm, but the intensity of the light at the different wavelengths is not given. A spectrometer from Avantes AvaSpec-2048 was used to get the number of counts of photons for each wavelength and the plot is shown in fig. 4.1. The spectrum was taken by holding the pick-up fiber of the spectrometer in the light reflected off a white piece of paper. This was done to prevent the spectrometer from saturating. The spectrum is not corrected for the sensitivity of the detector as a function of wavelength or the reflectivity of the paper.

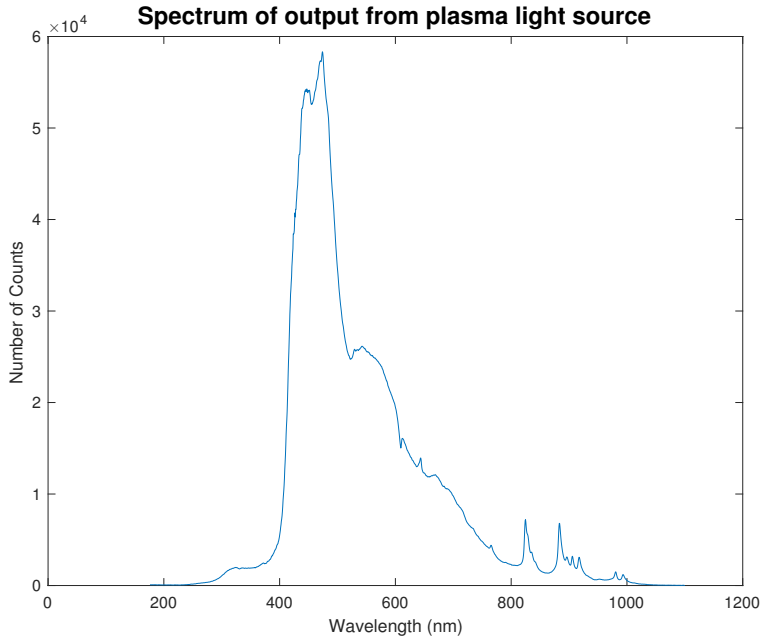

Figure 4.1: The spectrum of the light emitted by the plasma light source. The number of counts is plotted for each wavelength.

There is not much light that is emitted at a wavelength less than 250 nm or higher than 1000 nm. The actual wavelength range that allows one to perform wavelength dependent measurements is therefore reduced. In addition, the AOTF used here limits the range to go from 600 nm and the low intensity of the light source in the IR limits the range to 900 nm, at best. It is seen from fig. 4.1 that the LDLS emits most of the light in the range from 400 nm to 550 nm. This is a range that could not be utilized by the AOTF available, but there are other AOTFs that have an operating wavelength in the UV. The higher intensity could be utilized, but it is not very likely that the increase in optical power would be sufficient to give enough light for scatter measurements.

As previously mentioned, the output from the plasma enhanced white light source was coupled into a multi-mode fiber and connected to a reflective collimator. The collimator did not collimate the light perfectly because the fiber from the light source to the collimator is a multi-mode fiber and not a single-mode fiber. A UV-filter was placed after the reflective collimator and a lens was placed in the same lens tube in order to decrease the divergence angle of the beam. With a lens of focal length $f = 500\,\text{mm}$, the divergence angle was decreased to $1.05° \pm 0.03°$. The divergence angle was found by measuring the diameter of the beam on a millimeter paper at different distances to the paper. The beam radius is plotted

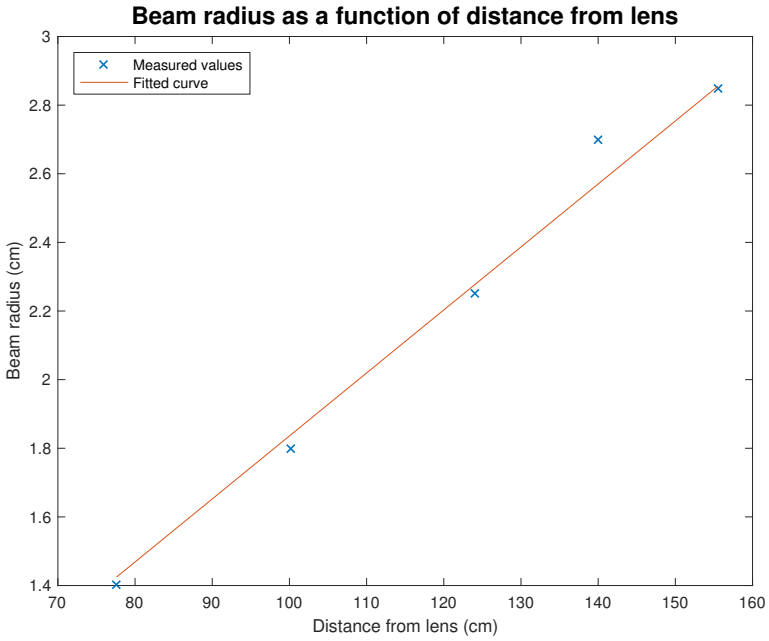

Figure 4.2: The beam radius is plotted as a function of distance from the lens with a fitted line. This is used to find the divergence angle of the beam going into the AOTF and what beam size it has at the entrance of the AOTF.

as a function of distance from the lens in fig. 4.2. The distance between the lens and the entrance of the AOTF is approximately 18 cm and the beam radius at the entrance of the AOTF is approximately 3.7 mm.

The orientation of the polarizer was optimized by looking at the output from the AOTF for different orientations of the polarizer. One wavelength was let through the AOTF and the spectrometer was used to measure the number of counts. The integrated number of counts for each orientation of the polarizer is shown in fig. 4.3. A fitted sine-curve is plotted to fit the measured values and to find the point at which the maximum intensity is. The best orientation of the polarizer is at 90.9° on the dial of the rotation mount, and the polarizer was set in this position for all the measurements to maximize the throughput of the system.

In an effort to find the optimal beam size, an aperture with an adjustable aperture size was inserted before the entrance of the AOTF. The aperture size was varied with the AOTF letting through light with a wavelength of 670 nm. The number of counts of the output from the AOTF was detected using the spectrometer and plotted in fig. 4.4 as a function of the aperture radius squared. The amount of light going out of the AOTF increases approximately

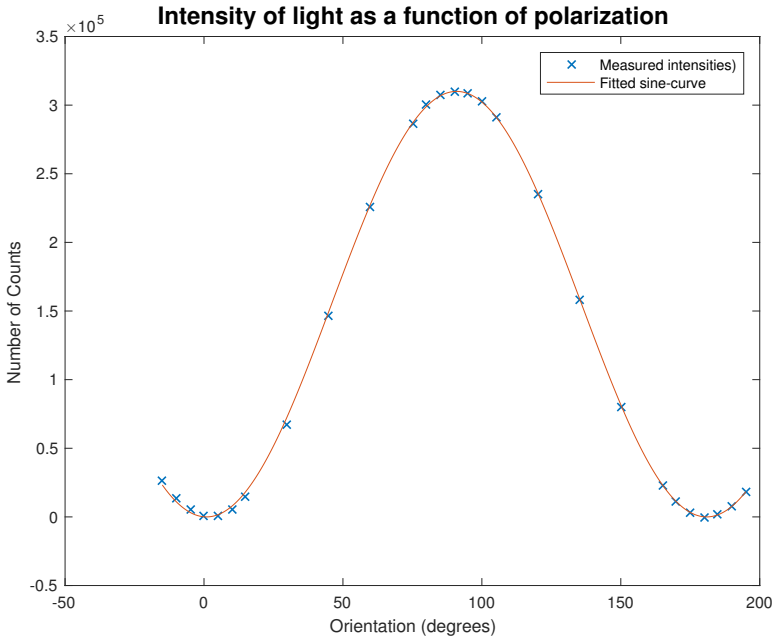

Figure 4.3: The measured values of the number of photons going out of the AOTF as a function of the orientation of the polarizer is shown as blue crosses. The fitted sine-curve to the data points is shown in a solid line. The fitted sine-curve gives an optimal orientation of the polarizer at 90.9°.

linearly with the radius squared until the beam radius is 2 mm, then it levels off. The beam radius should therefore be close to 2 mm for maximizing the throughput of the AOTF. A beam with a radius of more than 2 mm will lead to some of the light being lost, which will decrease the throughput of the AOTF.

A key figure to characterize the performance of the setup, is the relation between the intensity of light going into the AOTF and the intensity of light going out of it. For the system to be useful for waveguide loss measurements, the output of the AOTF has to be high enough to be detectable. Thus, the transmission of the AOTF should be as high as possible due to the intensity of the plasma light source being limited. Since the input is a broadband light source and the output is a narrow band of light, the Avantes spectrometer was used to compare the two intensities. The spectrum of the input light is plotted with the spectrum of the output from the AOTF in fig. 4.5. The intensity of the output light is found by integrating the number of counts of the peak. The counts in the input spectrum is integrated in the same wavelength range and the relation between the two integrals gives the throughput of the AOTF. This number was found to be between 14% and 11%, which is lower than the reported 40% from the manufacturer[27]. The light from the LDLS is not completely collimated and

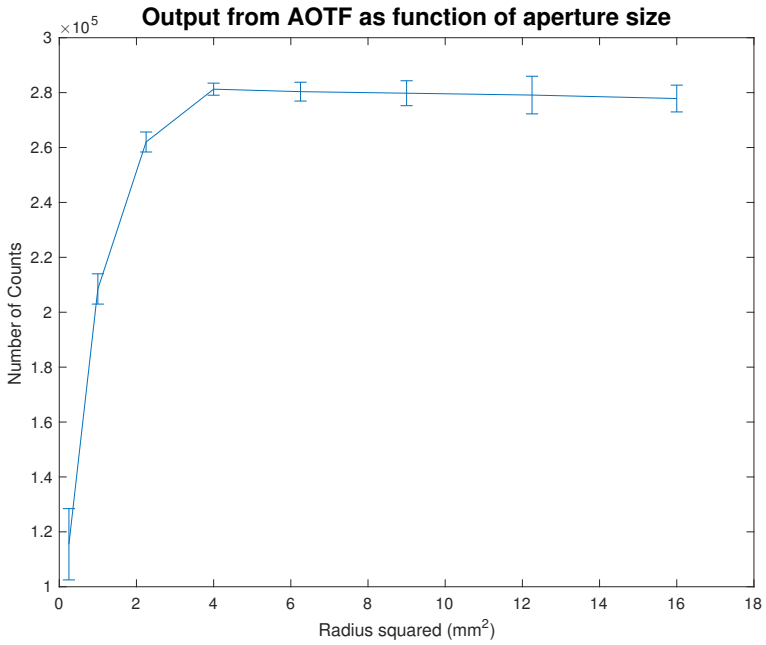

Figure 4.4: The integrated number of counts for the transmitted light from the output of the AOTF, plotted for each aperture radius squared. The output from the AOTF saturates at an aperture radius of approximately 2 mm.

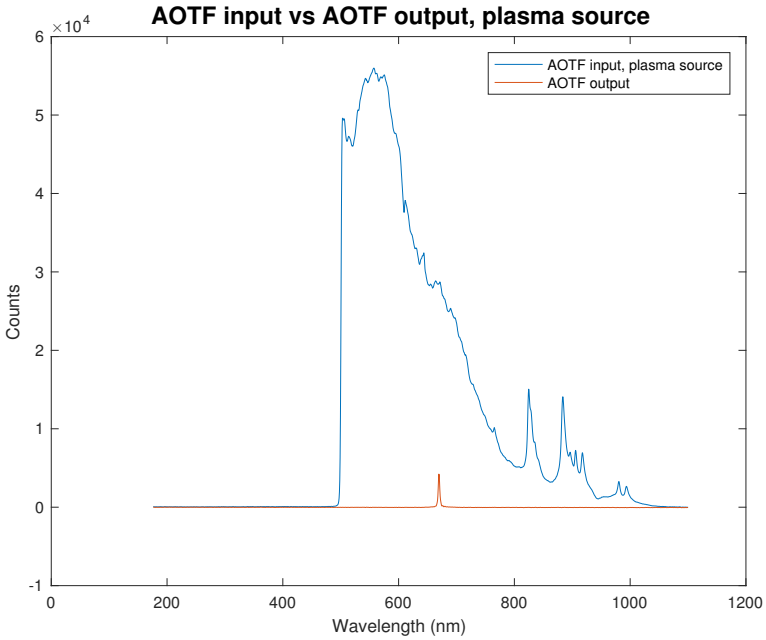

Figure 4.5: This figure shows the spectrum of the light entering the AOTF and the spectrum of the light exiting the AOTF. The relationship of the number of counts gives the throughput of the AOTF.

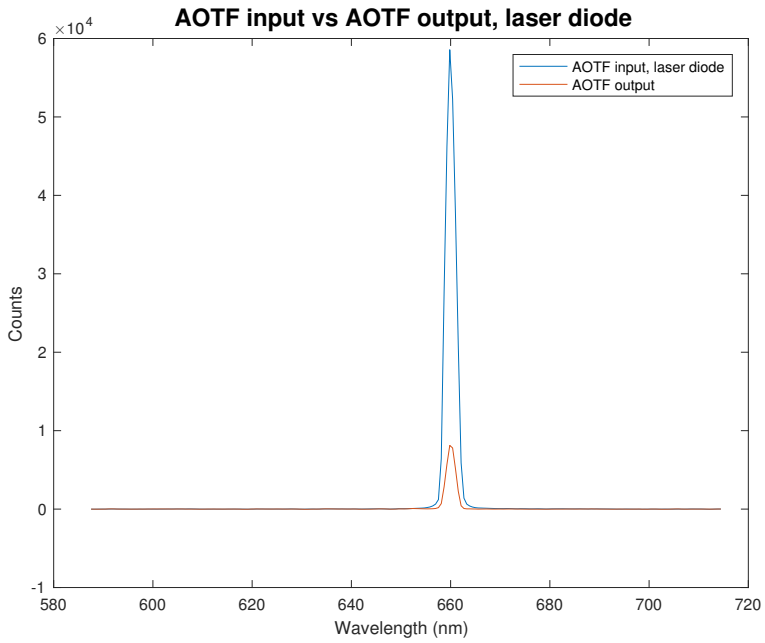

Figure 4.6: The spectrum of the light from a laser diode entering the AOTF is plotted with the spectrum of the output from the AOTF. The wavelength of the channel that is open in the AOTF is the one corresponding to the wavelength of the laser diode.

the beam radius is larger than 2 mm, meaning that some of the light is lost. This will lead to a lower throughput of the AOTF.

To see if the degree of collimation had a big effect on the throughput of the AOTF, the transmission efficiency was found in the same way as above, but now with a laser diode as a light source. The output of the laser diode was connected to a reflective collimator through a single-mode fiber that gave an output beam with a radius equal to 2 mm. The spectrum of the light sent into the AOTF and the spectrum of the output are plotted in fig. 4.6. The number of counts for both peaks were integrated between the same integration limits and compared. This gave a transmission efficiency of 12 %. It should be mentioned that the alignment of the pickup fiber with the input and output beams of the AOTF was challenging. The number of 12 % is therefore highly uncertain, but it is comparable to the transmission efficiency of the AOTF when the plasma source is used. One may therefore assume that the collimation of the light sent into the AOTF from the plasma source is satisfactory. In order to increase the intensity of the output from the AOTF, the input intensity should be increased without changing the collimation and the beam radius should be smaller.

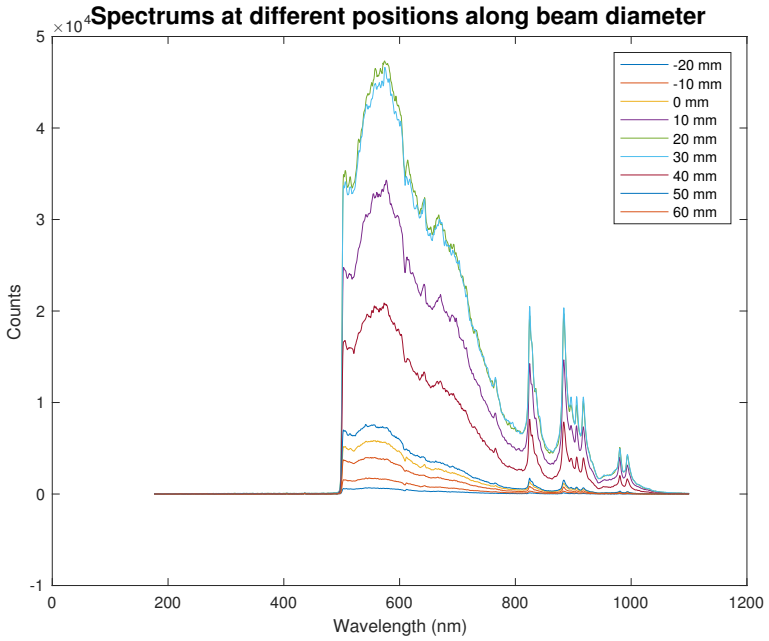

Figure 4.7: The spectrum of the light entering the AOTF at different positions along the diameter of the input beam. The number of counts is plotted for each wavelength and there is no change in the spectrum, only the intensity change.

In an effort to increase the intensity of the light coming out of the AOTF, the spatial distribution of the wavelengths and the intensity along the beam diameter was investigated. This was done to see if the intensity distribution of the beam going into the AOTF is not highest in the center of the beam. Since the beam radius at the entrance of the AOTF is larger than 2 mm, the outer part of the beam is lost. If this is where the beam is most intense, it would lead to a decrease in the transmission efficiency of the AOTF. The spectrums of the light at different positions along the diameter of the beam are shown in fig. 4.7 and there are no significant changes in the wavelength distribution in the beam, but the intensity change. The integral of the counts for each wavelength gives the intensity of the beam and is shown in fig. 4.8. This shows that the beam has the highest intensity in the center of the beam, at a position 24 mm. The beam profile was measured further away than 18 cm, but this was to be able to see the profile of the beam more clearly.

In order to get a high throughput of the AOTF as possible, the collimation of the input beam and the alignment of the setup have to be optimized. The collimation of the beam is good and the alignment tool works as it is supposed to. There is some room to move the lens tube attached to the reflective collimator, but by detecting the output from the AOTF, the

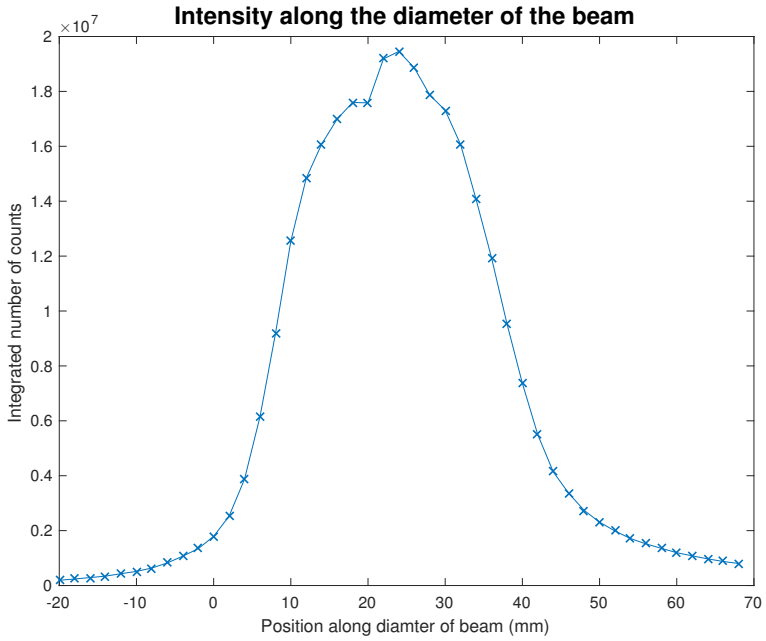

Figure 4.8: The intensity (integrated number of counts from the spectrums) of the light at each position of the beam is plotted. The beam has the highest intensity at the center of the beam.

position of the lens tube can be optimized to give the maximal output from the AOTF. The major limiting factor in the setup is therefore the intensity of the LDLS. It was believed that the LDLS emitted light in the IR, up to 2000 nm, but it was shown that the intensity here was quite low. This also limited the range in which it was possible to do wavelength dependent measurements of the losses. The AOTF is a dual system with two crystals, and it can filter light with a wavelength up to 2000 nm. To utilize the possibilities of the AOTF and the setup designed, a more powerful white light source should be used which has a higher intensity, also in the IR.

Other light sources were tested in an effort to get more light out of the AOTF. It was attempted to collimate the light from a halogen light bulb and a spectrometer light bulb. Both light sources emit a lot of power, but in a wide direction. A pinhole was placed in front of the light bulb and two lenses at different positions were used to collimate the light. The light was collimated, but not well enough to give a detectable output from the AOTF. Even though the total power of the light bulbs are high, the amount of light that is emitted in a narrow angular direction is not that high, thus not yielding a higher output of the AOTF.

4.1.2 Output from AOTF

The output from the AOTF was detectable when using the LDLS as a light source, but with a low intensity. It was therefore necessary to collect as much of the light coming out of the AOTF as possible. The AOTF came with a collimator connected to a fiber. The collimator fits into the output piece of the AOTF, collects the output light and directs it into the fiber. The fiber that came with the AOTF is a Thorlabs GIF625 fiber with a core diameter of 62.5 µm. A different configuration of collecting the output from the AOTF was tested to see if it was possible to send more light into the waveguide. A funnel collimator connected to an Ocean Optics P400-2UV/VIS fiber, which has a core diameter of 400 µm. The throughput of these two fiber setups was tested, and the funnel collimator with the Ocean Optics fiber let through 65 %, while the collimator and the Thorlabs fiber let through 45 % of the light.

The fact that the Ocean Optics fiber gave a higher throughput than the Thorlabs fiber is not surprising, considering the core diameter of the Ocean Optics fiber being larger and therefore able to collect more light. However, a fiber with a large core diameter as 400 µm is hard to couple into a thin film waveguide with a thickness of a few hundred nm. Even though the throughput of the funnel collimator and the Ocean Optics fiber was higher than for the collimator and fiber that came with the AOTF, the last collimator and fiber configuration was chosen because not as much light was lost when coupling into the waveguide.

The fiber at the output of the AOTF was coupled to a bare end fiber which was mounted for coupling into the waveguide. Both the coupling between the two fibers and the transmission in the bare end fiber will limit the total amount of light that is coupled into the waveguide. Since there is a limited amount of light output from the AOTF when the LDLS is used, the coupling between the two fibers and the throughput of the bare end fiber should be as high as possible.

4.2 Thin Films

In order to have a waveguide to measure the wavelength dependent losses of, three different materials were tested. The films were made by spin coating and the details of the manufac-

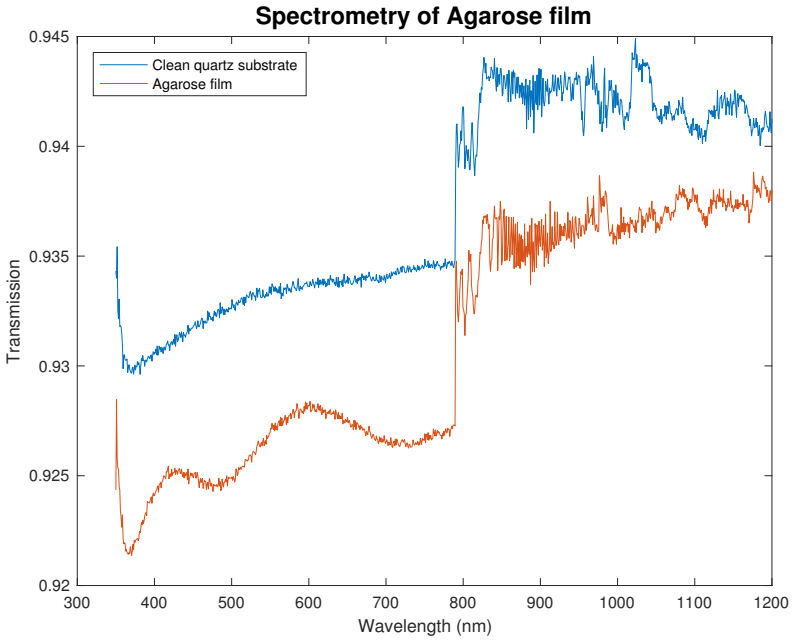

Figure 4.9: The transmission spectrum of the Agarose film is shown with the transmission spectrum of a clean quartz substrate. It is possible to see the interference fringes of the Agarose film and use this to calculate the thickness of the Agarose film.

turing of all three films are explained in the following section.

4.2.1 Agarose Film

The process of making thin films of Agarose proved to be challenging. It was difficult to keep the temperature of the Agarose solution and the substrate at the same level for each try, and at the same time change the rotation speed to find the optimal setting. Spectrophotometry of the films that were made, was performed on an Olis Spectrophotometer and a transmission spectra is shown in figure fig. 4.9. The interference fringes show that the film might have the right thickness to guide waves.

The temperature of the Agarose solution was challenging to control and it seemed to be a matter of luck more than skill that led to a film with a thickness that could support guided modes. For the Agarose film with its transmission measurement presented in fig. 4.9, several other films were made with the same rotation speeds and they did not show any interference fringes, thus not having the same thickness. In addition, the Agarose films detached from the substrate easily, making it difficult to polish a clean end for end-fire coupling.

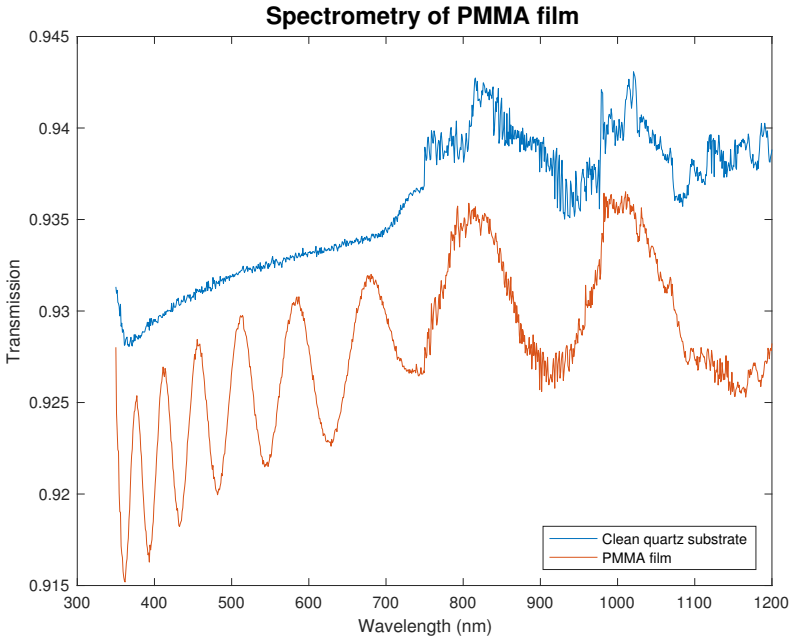

Figure 4.10: The transmission spectrum of the PMMA film is shown with the transmission spectrum of a clean quartz substrate.

4.2.2 Polymethyl Methacrylate Film

The thickness of the PMMA films made, was found by spectrophotometry on the same Olis Spectrophotometer as above. The transmission spectrum is shown in fig. 4.10 and the spacing of the interference fringes can be used with eq. (2.15) to calculate the thickness of the film. The refractive indices of the PMMA film at the wavelength of the fringes are found in [28]. This gave a thickness of

$$d = 1370\,\text{nm} \pm 47\,\text{nm}.$$

The film is thinner than one would expect from the approach selected from the recipes from NanoLab. By using eq. (2.14), one find that the PMMA film can support approximately 2 modes and it was polished to reveal a clean edge for end-fire coupling. The film was first wet-polished, but this lead to the film peeling off the edges where it had been in contact with water. The film was therefore dry-polished. The attempts to couple into the film was not successful. Possible reasons for this may be a poorly polished edge and that the refractive index of the quartz substrate and the refractive index of the PMMA are close. This could lead to the light being lost into the substrate which would lead to higher losses in the waveguide and not possible to see a guided streak.

4.2.3 Polystyrene Film

The thin film waveguide made of Polystyrene (PS) had to be characterized to find out if the thickness was suitable to support modes. Spectrophotometry was also performed on this film and the transmission spectrum is shown in fig. 4.11. The interference fringes in the transmission measurement from the PS film were used with eq. (2.15) and the refractive indices to calculate the thickness of the films. The refractive indices of the PS at the wavelengths of the peaks are found in [28]. The peak at 365 nm could not be used, due to the refractive index of PS is not being known at this wavelength. This gave a thickness of

$$d = 412\,\text{nm} \pm 10\,\text{nm}$$

The thickness should also be used to see how many modes the film can support and this is calculated by using eq. (2.14). Using the appropriate refractive indices at a wavelength equal to 600 nm gives $m = 0$, and the film can only support its fundamental mode (corresponding to $m = 0$). The film was then polished to have a clean edge suitable for end-fire coupling and it was possible to couple into the film as illustrated in fig. 4.12.

The PS waveguide was made by taking a piece of a plastic box and dissolving it. This was a crude process that most certainly lead to a waveguide containing impurities, thus increasing the losses. This turned out not to be a big problem, since the losses were not too high and it was possible to guide waves in the thin film. Also, the losses cannot be too low, otherwise the intensity of the light scattered out of the surface of the waveguide would be too low to detect.

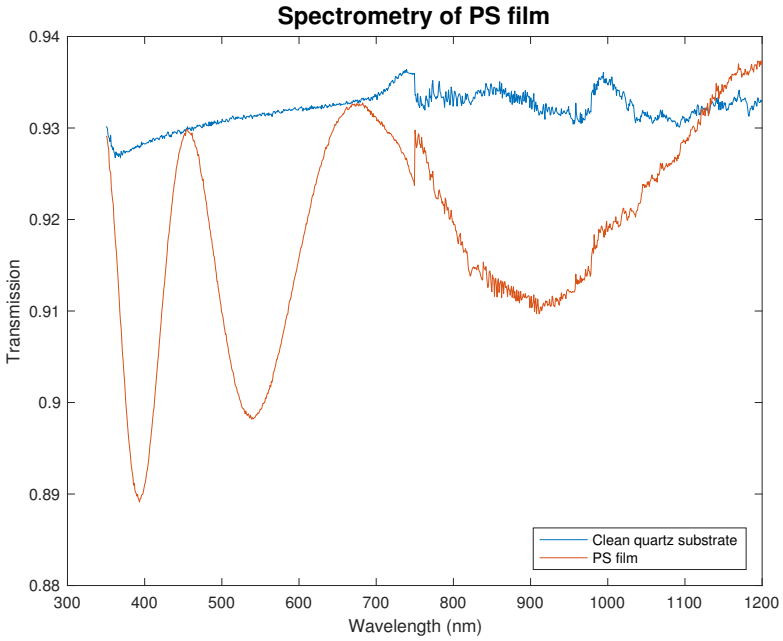

Figure 4.11: The transmission spectrum of two different PS films is shown with a the transmission spectrum of a clean quartz substrate as reference. The interference fringes of the PS films are used for finding the thickness of the PS films

4.3 Losses in Polystyrene Thin Film Waveguide

The reason for making a setup with a different light source than the white light laser, was to use it to measure wavelength dependent losses is waveguides. The results from the using the different setups to find the losses in the PS waveguide is presented in the following sections.

4.3.1 Laser Driven Light Source

The output light from the AOTF after the collimator and the fiber is approximately 5 µW at 650 nm. It is possible to detect the light with the spectrometer or the Silicon detector when the light is directed straight into the pick-up fiber. When the output from the AOTF is coupled into the waveguide, the amount of light scattered from the surface of the waveguide is too low to be detected by the spectrometer. Experience has shown that a substantial part of the light is scattered out at the coupling spot, as one may also see from fig. 4.12. A laser diode was coupled to the bare end fiber which was used to couple into the waveguide. The pick-up fiber was placed over the coupling spot and it was verified that there was a detectable signal at this position. Then, the output from the AOTF was coupled into the bare end fiber without moving the bare end side of the fiber and keeping the pick-up fiber in the same position.

It was not possible to detect a signal from the output of the AOTF.

The sensitivity of the spectrometer is not good, and in an effort to get a higher signal-to-noise ratio, the RF signal to the AOTF was modulated for it to be used with a lock-in amplified detector. This was done in an effort to see if a detectable signal of the light scattered out of the waveguide was obtainable when using the LDLS with the AOTF. As explained above, a laser diode was coupled into the bare end fiber and light was coupled into the waveguide. The detector was then moved to the place where there was maximal signal from the scattering. Then, the laser diode was removed and the output for the AOTF was coupled into the bare end fiber, ensuring the light was still coupled into the waveguide. When placing the detector at the spot which gave maximal signal for the laser diode, there was no detectable signal and it was concluded that the setup used with the LDLS does not give enough light for it to be used for scatter measurements of losses in waveguides.

To give an estimate of how much light that has to go through the AOTF, a laser diode that was modulated with a signal from the lock-in amplifier was turned down to where the signal of the scattered light from the waveguide could just barely be detected by the lock-in amplifier. This gave a signal of approximately 100 mV at the end of the bare-end fiber and an output from the fiber coupled into the bare-end fiber of approximately 0.9 V. This will give an idea as to how intense the light source has to be, by taking into account the throughput of the AOTF and how much of the output that is collected into the fiber.

The numbers presented above are for a narrow band of wavelengths, but it is possible to open multiple channels at the same time to increase the bandwidth of the light let through the AOTF, thus giving a higher number of photons going through. This was done with the LDLS to see if there was a detectable signal, but it was not. However, a stronger white light source may give a sufficient number of photons through the AOTF when broadening the bandwidth. This could allow for preliminary measurements of losses in waveguides.

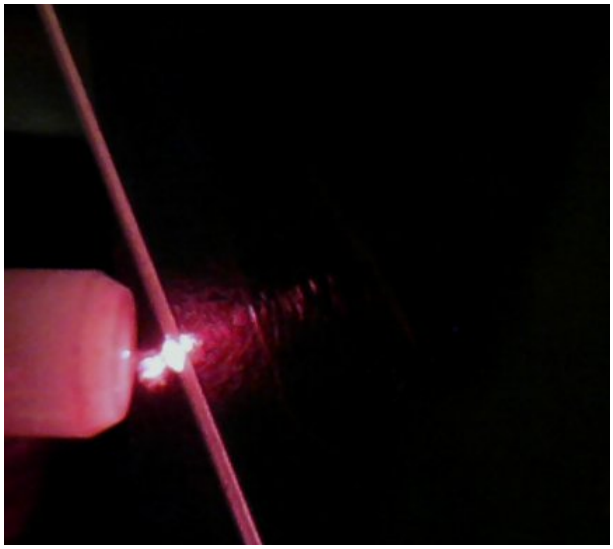

Figure 4.12: This is an image taken of the PS waveguide coupled into using light with a wavelength of 650 nm from the white light laser, filtered through the AOTF. There is some scattering at the coupling spot, but a visible streak of light is going through the waveguide.

4.3.2 White Light Laser and Spectrometer

Due to the intensity of the LDLS being too low, the white light laser that goes with the AOTF was used as a light source. This gave a signal that could be detected by the Avantes spectrometer and several manual scans of the surface of the waveguide was performed, as described in section 3.3.

First, the waveguide was coupled into using just the bare end ferrule of the fiber going from the collimator. The fiber has a numerical aperture of 0.275, but it was possible to couple into the waveguide when the end of the fiber was close enough to the edge of the waveguide. The image in fig. 4.12 shows that there is some scattering at the coupling spot, but a distinct streak is possible to see going through the waveguide at an angle with respect to direction of the light going out of the ferrule.

All eight channels of the AOTF was turned on and a scan of the surface of the waveguide was performed using the spectrometer. The wavelengths that was let through the AOTF was 600 nm, 650 nm, 690 nm, 730 nm, 770 nm, 810 nm, 850 nm and 890 nm. These wavelengths were chosen based on the wavelength range of the AOTF with the LDLS. Even though it turned out that the LDLS could not be used for loss measurements, the wavelength range

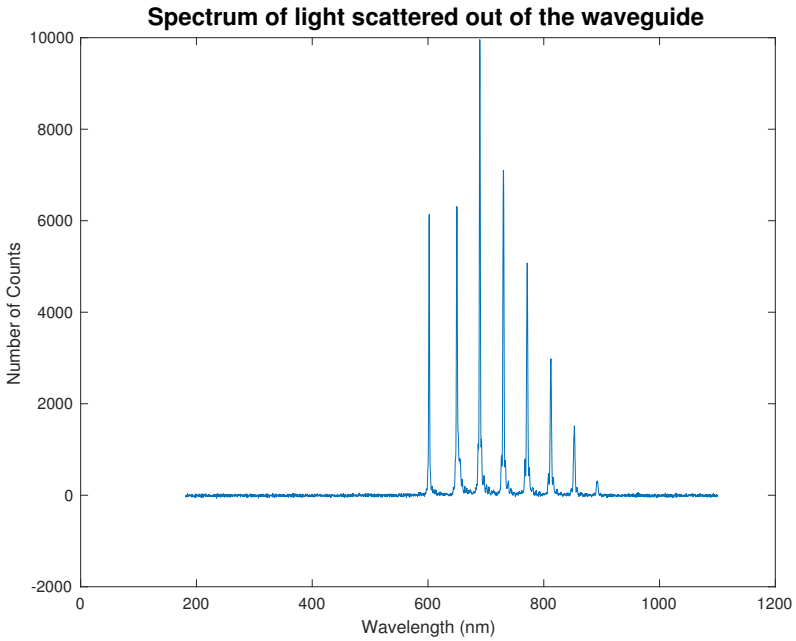

Figure 4.13: This is a typical spectrum of the light scattered out of the surface of the waveguide when using the white light laser as a light source. The number of photons at each wavelength is plotted as a function of wavelength and there can be seen eight different peaks, corresponding to the eight wavelengths that are let through the AOTF.

of the manual scans was selected before this was verified. The wavelength range was therefore limited to less than 900 nm for the measurements to possibly be compared with the loss measurements using the LDLS.

The scan of the light scattered out of the waveguide gave a spectrum for each point on the surface. The resolution of this scan was 0.05 mm in the x-direction and 1 mm in the y-direction. The resolution of the scan across the guided streak has to be small enough to be able to image the profile of the streak. A typical spectrum taken at a point at the surface of the waveguide is shown in fig. 4.13. There are eight distinct peaks at each of the eight wavelengths that were chosen to be let through the AOTF, all with a FWHM of approximately 3 nm. To get the intensity of the light from each peak, the number of counts for each wavelength was integrated. For each point in the scan and for each wavelength, the integrated number of counts is found. The integrated number of counts at each position is plotted in a surface plot, as shown in fig. 4.14. This is the surface plot for the signal at 600 nm, but the surface plots for the other wavelengths look similar. The surface plot is made to see if the scanning gives a plot that agrees with the image of the light coupled into the waveguide, for

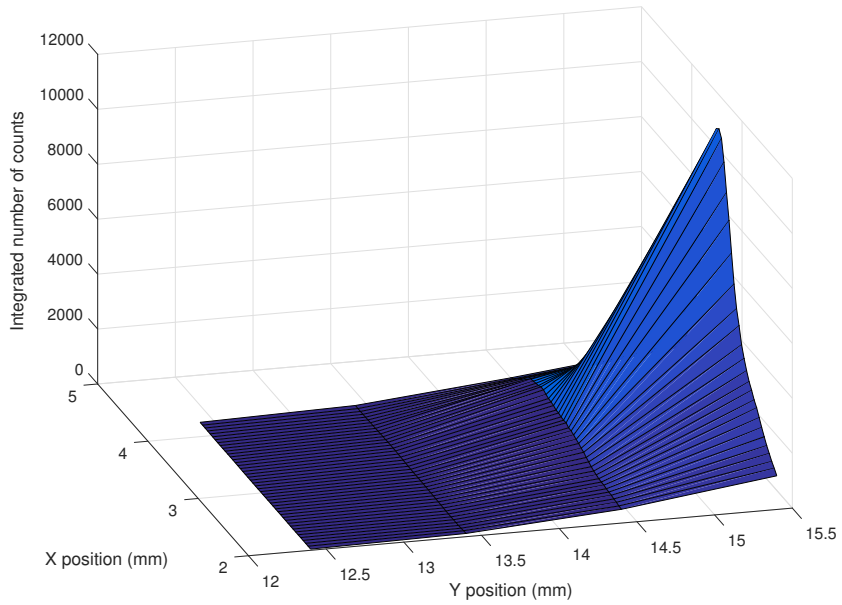

Figure 4.14: The integrated number of counts at each measuring point is plotted to create a surface plot. This plot shows the integrated number of peaks for light with a wavelength of 600 nm, but the other surface plots look similar.

instance, if the light goes on an angle with respect to the x- and y-directions. The surface plot agrees with what one would expect to see from the image taken of the streak in fig. 4.12.

For each scan along a line of constant y, the maximum value of the integrated number of counts is found and its corresponding x-position. Since the streak goes on an angle with respect to the x- and y-axes, the x and y- positions of the maximum number of counts are used to find the distance, s, which is given by the Pythagorean theorem, $s = \sqrt{x^2 + y^2}$. The maximum of the integrated number of counts are plotted as a function of s, as shown in fig. 4.15. The loss in the waveguide for each wavelength was found by fitting an exponential curve to each of the curves in fig. 4.15 and using eq. (2.17). Similar scans were performed at a later occasion, but using the drawn fiber to couple into the waveguide. The losses were found in the same way, by fitting an exponential to the plots in figs. 4.16 and 4.17.

The three different scans gave one loss value for each of the eight wavelengths. The loss values for each wavelength was averaged and are plotted as a function of $1/\lambda^4$ in fig. 4.18. The loss is plotted as a functions of $1/\lambda^4$ to more clearly see a straight line, as one would expect

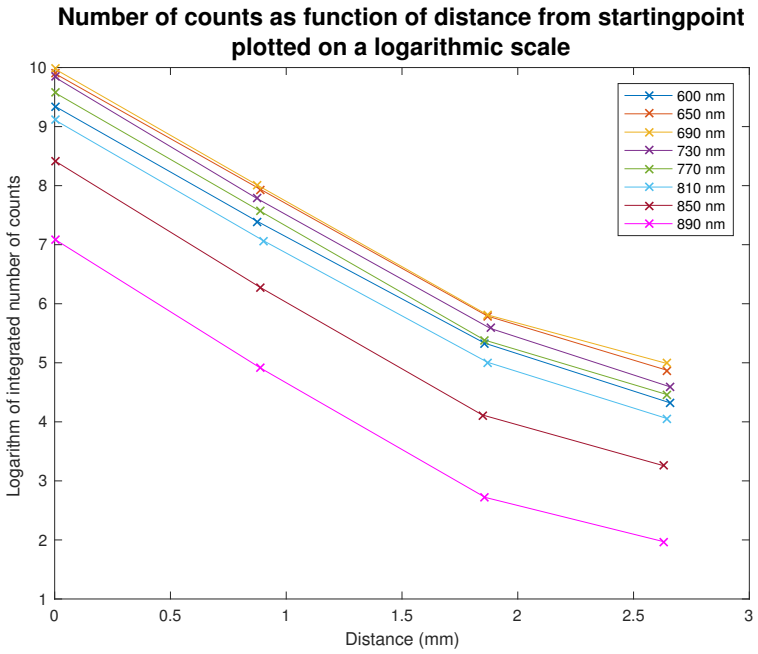

Figure 4.15: The number of integrated counts is plotted as a function of distance from the point of the first maximum value found. The intensity can be seen to follow an exponential decay. This plot is obtained from the scan perferomed when the light was coupled into the waveguide using the bare end ferrule.

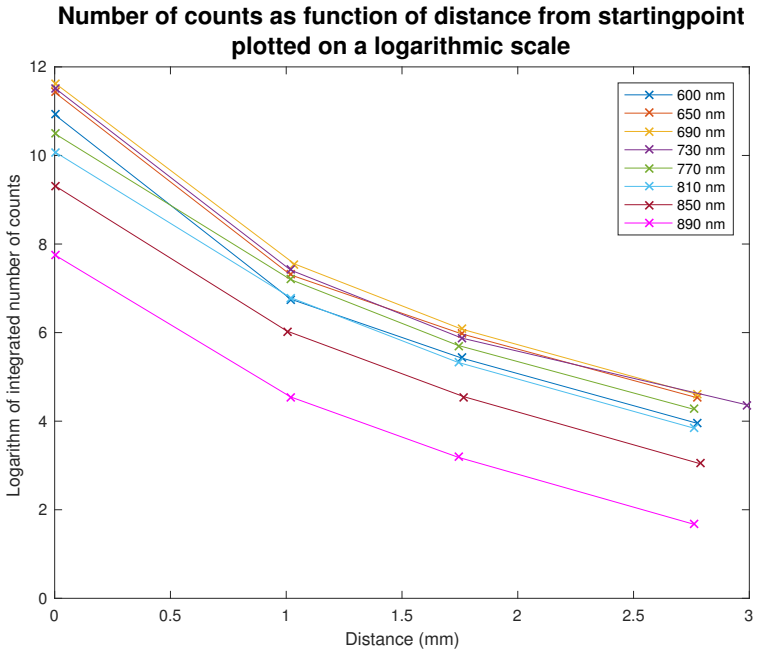

Figure 4.16: The integrated number of counts is plotted as function of distance. The plot is used to find the loss of the waveguide for the different wavelengths. This plot is obtained from the data from the first scan when using the drawn fiber to couple into the waveguide.

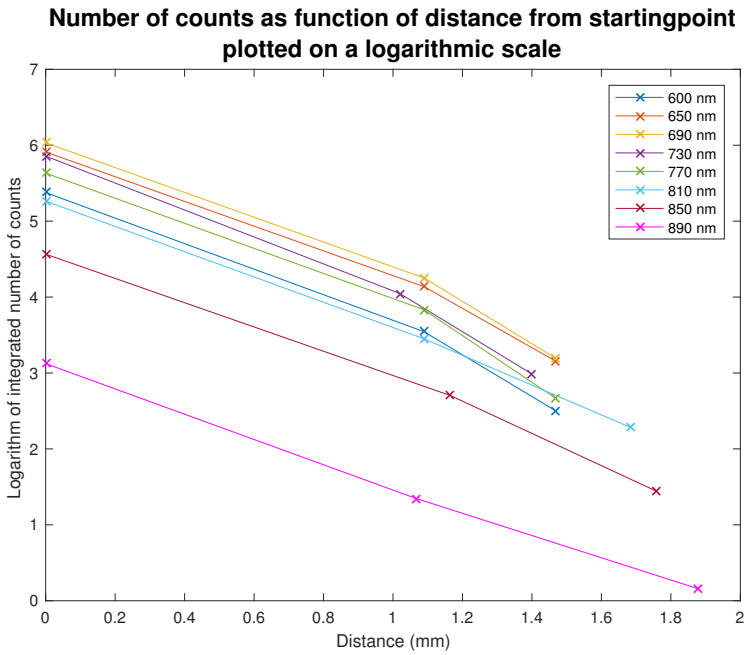

Figure 4.17: The integrated number of counts is plotted as function of distance. This is plotted based on the data obtained from the second scan when using the drawn fiber to couple into the waveguide

from the assumption that the loss decays as $^1/_{\lambda^4}$. The losses do not follow a straight line that decay for increasing wavelengths. The range of wavelengths is short and it would have been easier to see if the trend of the loss over a larger range of wavelengths.

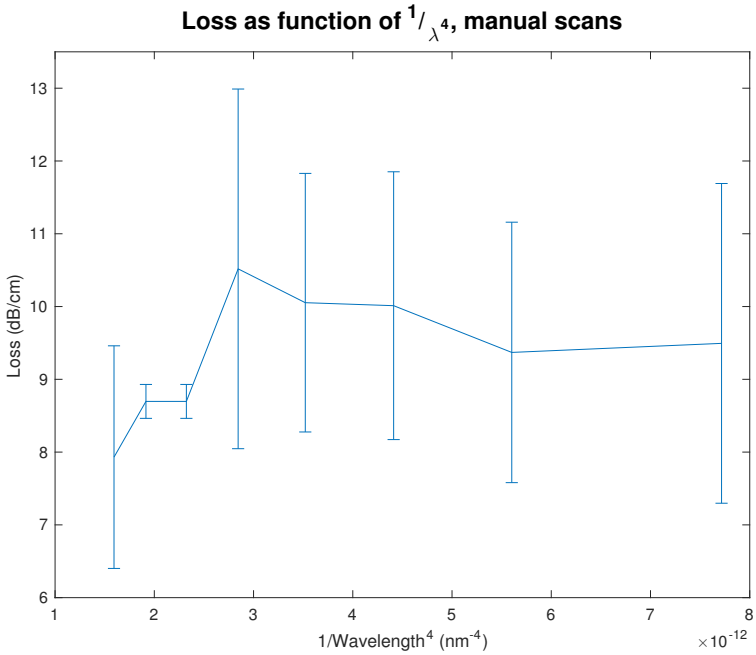

Figure 4.18: The average loss values is plotted as a function of $^1/_{\lambda^4}$. The values should follow a straight line, but it does not all though it is possible to fit a straight line within the error bars of the loss values.

It is easy to argue that the resolution if the manual scanning should have been higher in the y-direction. The way it was done here, gave only four points for fitting the exponential curve. If there had been more points, it would be possible to give more accurate values for the losses. In addition, the big steps in the y-direction gave a low intensity for the scans along the lines of constant y that were far from the coupling spot.

The advantage of using a spectrometer when scanning the surface of the waveguide is that it took only one scan to get the intensity distribution of all the eight wavelengths. However, the sensitivity of the spectrometer is low and the signal to noise ratio is low when the signal gets weak. This made it hard to get information about the scattering further from the coupling spot. As the intensity of the light got lower, further away from the coupling spot, the integration time on the spectrometer was increased, but this did not improve the signal to noise ratio.

4.3.3 White Light Laser and Lock-in Amplification

Using a detector with a lock-in amplifier gives a higher signal-to-noise ratio, meaning that a signal with lower intensity can be detected. This enables the scans to be longer, as well as the automated scan process enables the resolution of the scans to be higher. This results in data where there are more points to fit to the linear curve, increasing the accuracy of the loss values.

The white light laser was used with the AOTF to get a detectable output which could be coupled into the PS waveguide. The RF signal was modulated with a lock-in amplifier to get a signal-to-noise ratio that was as high as possible. The wavelengths chosen for the loss measurements was the same as the wavelengths chosen for the manual scans using the spectrometer, in order to compare the two methods, but two wavelengths of 1000 nm and 1100 nm was added.

The output from the AOTF was coupled into the PS waveguide using the bare end fiber and is shown in fig. 4.19. The scans gave surface plots of the intensity of the light scattered out

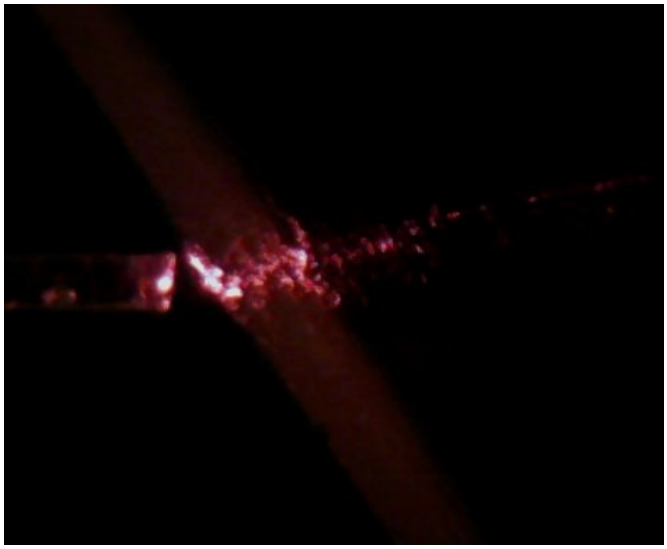

Figure 4.19: Light from the white light laser is filtered through the AOTF and coupled into the PS waveguide using end-fire coupling. The light has a wavelength of 650 nm and it is possible to see the scattering from a streak that is guided

of the surface of the waveguide, similar to the surface plot from the manual scans using the spectrometer. The detector used with the lock-in amplifier measures the intensity of the light and converts it to a voltage, yielding that the voltage is plotted as a function of x- and y-position at the surface. One of these plots are shown in fig. 4.20.

The maximum value for each scan along a line of constant y is found with its corresponding x-position. The logarithm of the maximum voltage is plotted as a function of distance, $s = \sqrt{x^2 + y^2}$. The plots for the different wavelengths are given in figs. 4.21 and 4.22. The solid lines in blue are the loss values obtained by fitting the straight line to a selection of the data points and the green dashed lines are the loss values obtained by fitting to all of the data points.

Some of the scans had humps in them, as one can see in fig. 4.21e, for example. These humps could be caused by scattering centers. The selection of points have been made to avoid the peaks in the intensity in the plots which contain these features. The loss values for both the linear fit to all the data points and the selected data points are given in table 4.1 as well as the relation between the intensity of the hump and the peak intensity of the plot.

The humps in figs. 4.21a and 4.21b are small compared to the humps in the plots for the

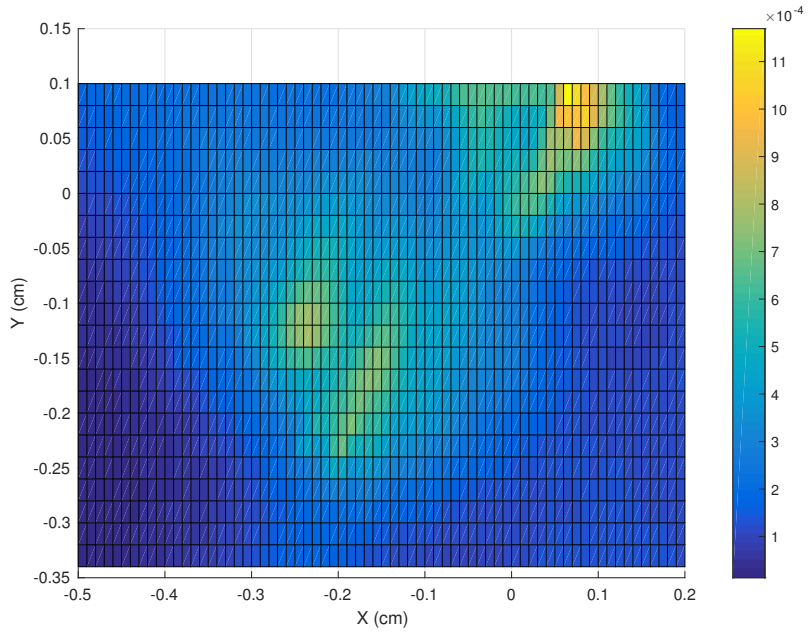

Figure 4.20: The top view of a surface plot of the waveguided streak in the PS thin film. The voltage detected by the lock-in amplifier is plotted as a function of x- and y-position and the scale for the voltage is given by the color bar on the right. It can be seen that the streak goes on an angle with respect to the x- and y-directions, indicating that the light is coupled into the waveguide. The light has a wavelength of 850 nm.

longer wavelengths. The fitted curves in these two plots (blue lines) have not omitted the humps, since they are small compared to the intensity of the rest of the signal. This will lead to a slight decrease in the loss values obtained for these two wavelengths.

Figure 4.21c does not show a hump and the selected data is the last part of the scan. The first part of the scan is believed to be a region where mode stripping occur and it is therefore avoided. The scans were started a distance away from the coupling spot to avoid the mode stripping region, but it is possible that this region has not been completely avoided.

The scattering center will decrease the total amount of light that is going through the waveguide, but the loss before and after the scattering center should be the same. This means that the intensity should follow the same slope before and after the humps in the plots in figs. 4.21 and 4.22. The two different slopes are similar in figs. 4.21d to 4.21f, 4.22a and 4.22b. One important objection to these fitted curves is that the curves in the beginning of the plot are believed to be in the mode stripping region and the fitted curve after the hump may be fitted to values that are still affected by the light from the scattering centers. Both the mode

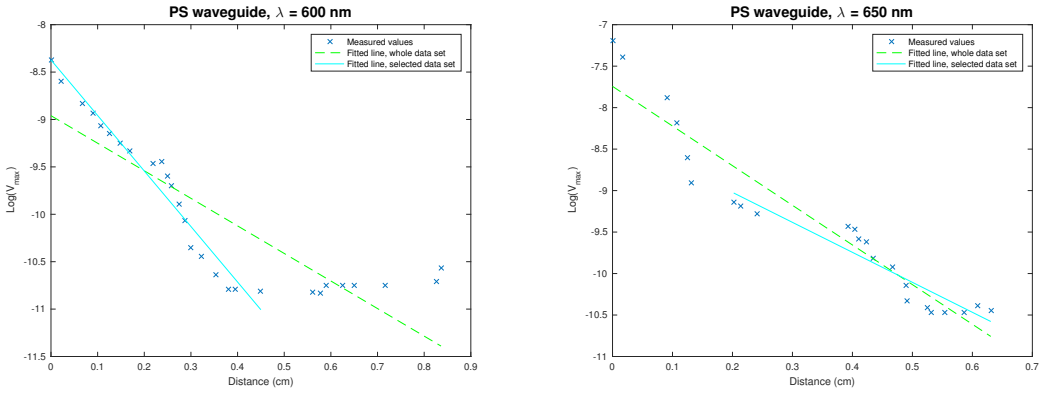

(a)

(b)

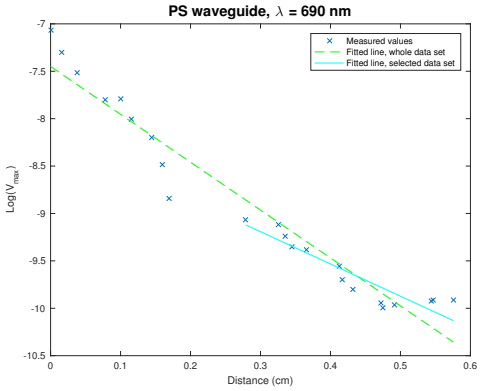

(c)

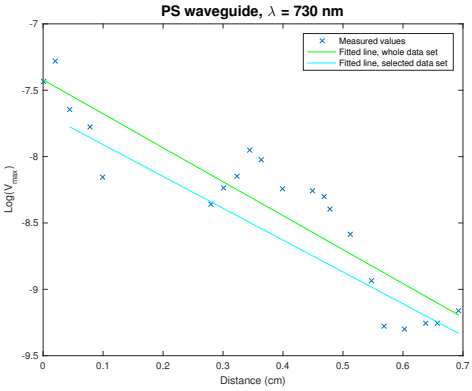

(d)

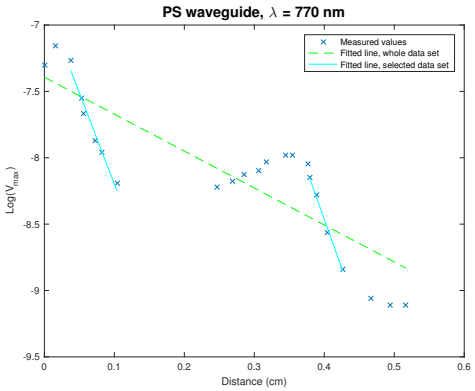

(e)

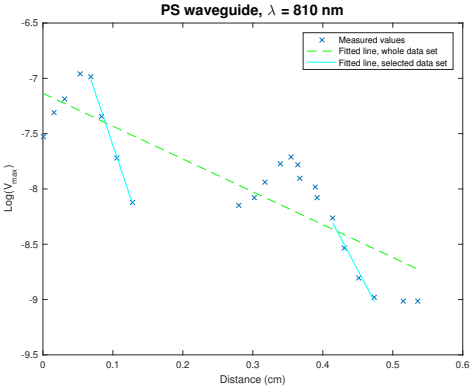

(f)

Figure 4.21: The detected signal is plotted on a logarithmic scale as a function of distance. Linear curves are fitted to the measured data to find the losses in the waveguide. The plots shown in this figure is for the scans of the waveguide illuminated with light with a wavelength of 600 nm,650 nm, 730 nm, 770 nm, and 810 nm.

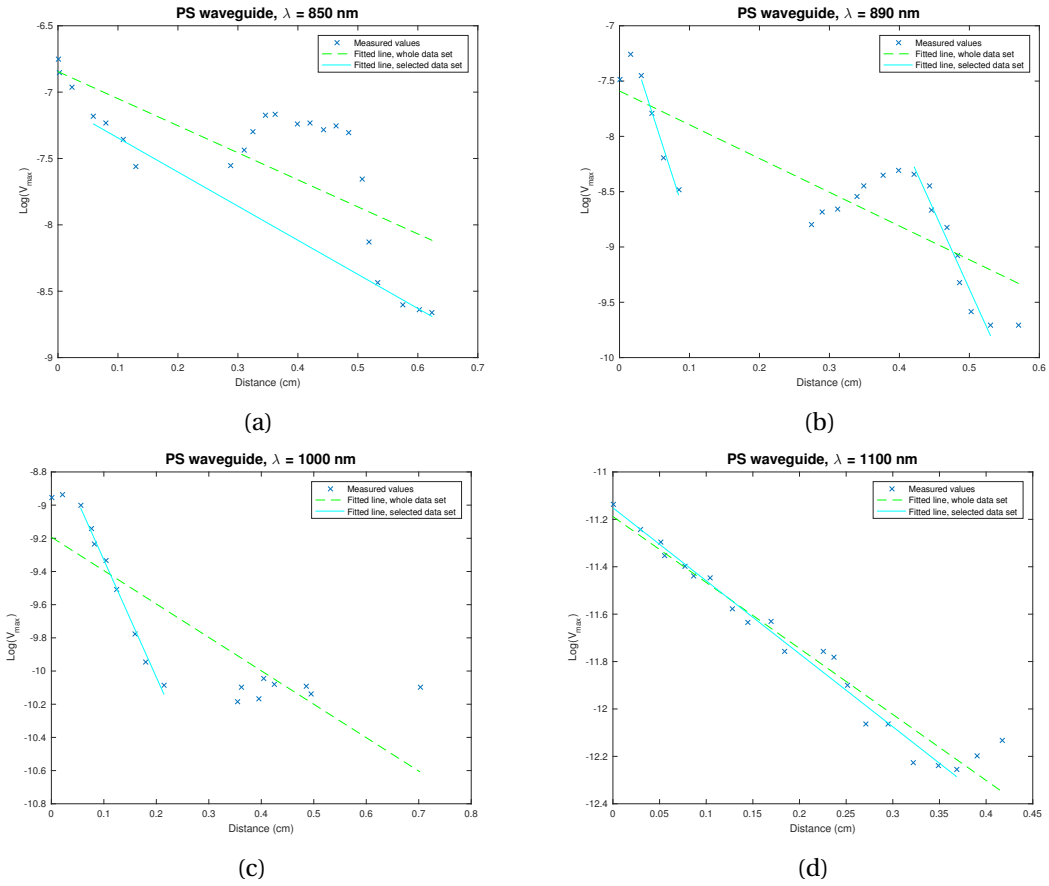

Figure 4.22: The logarithm of the detected signal of the light scattered out of the waveguide is plotted as a function of distance along the guided streak. Lineat curves are fitted to the data points to find the losses in the PS waveguide for the wavelengths 850 nm, 890 nm, 1000 nm, and 1100 nm.

stripping region and the region close after the hump will lead to an increase in loss values.

Table 4.1: The losses in the PS waveguide for different wavelengths, measured using the white light laser as a light source. The losses when fitting to all the data points and to a selected set of the data is shown. The relation between the intensity of the hump and the peak intensity of the plot is also given.

Wavelength (nm)	Loss (dB/cm) fit to all data	Loss (dB/cm) fit to selected data	Hump	Hump intensity/ peak intensity
600	12.6	25.4	Yes	0.31
650	20.7	15.7	Yes	0.10
690	21.9	14.8	No	
730	11.1	10.4	Yes	0.51
770	12.1	60.0	Yes	0.43
810	12.9	51.7	Yes	0.47
850	8.8	11.2	Yes	0.66
890	18.1	61.4	Yes	0.35
1000	6.4	30.7	No	
1100	12.1	13.4	No	

Figures 4.22c and 4.22d does not show a hump and it was not necessary to avoid a particular part of the data set. The blue line in fig. 4.22c is fitted to the first part of the data set. This was done because the later part of the scan is believed to be noise where there is no guided streak. The first region is believed to be in the mode stripping region which will give a higher loss value than the actual losses. However, one should expect a change in slope when the data is outside the mode stripping region, but this does not happen. This may be because there was no mode that outlasted the mode stripping region and there was only noise that was detected after this.

The blue fitted line in fig. 4.22d is fitted to almost the whole part of the data set, only omitting the last points that show an increase in the detected signal. This plot shows a constant slope over almost the whole the data set and the fitted blue line fits well with the measured values.

The humps in some of the scans may be caused by scattering centers. As previously stated, the PS waveguide was made by dissolving a plastic box. Possible contamination may have been introduced when the plastic box was cut or from particles that were on the surface of the plastic. This was a crude process that could only result in a waveguide with low purity.

The dissolved polystyrene was not filtered, which would have made the waveguide less contaminated.

The data for the 600 nm to the 1000 nm was performed with the light being coupled into the waveguide at the same spot and with the same angle between the waveguide and the bare-end fiber. The 1100 nm measurement was performed with the light coupled into the waveguide at a different spot, and it could be that the guided light is going through the waveguide in a region where there are no scattering centers or impurities.

The light with the different wavelengths will experience different indices of refraction. This leads to the light being bent at different angles and thus being guided at different positions in the waveguide. The refractive indices of the PS waveguide at the different wavelengths are found in [28]. The refractive index of the PS is slowly decaying as a function of wavelength, yielding that the difference in the refracted angle between the light with a wavelength of 600 nm and 1100 nm is 0.2°, when the light is coupled into the waveguide at the same angle for all the wavelengths. A rough estimate of the position of the scattering center being approximately 10 mm from the coupling spot yields the result that the the guided light with different wavelengths span over a distance of approximately 70 µm at the estimated position of the scattering center. Particles and grains in the film is expected to be tenths of microns, meaning that all the different wavelengths are able to hit the impurity in the film. There should be humps in all the scans, except for the one with $\lambda = 1100$ nm, but a more thorough study of the characteristics should be carried out.

It should be noted that some of the loss values are high, especially the loss values for light with wavelength 770 nm, 810 nm, 890 nm and 1000 nm. The curves in these figures have been fitted to data points that are either in the mode stripping region or close to the hump in the plot. This results in losses that are higher than what they actually are.

Although the scans of the scattered light in the PS waveguide for different losses is not believable due to the humps in the scans, it also revealed that the setup can be used to find other traits of a waveguide. The humps may be caused by a grain or other impurities, but

these few measurements show that the setup with the white light laser, the AOTF and the lock-in detection allows for investigation and characterization of impurities in a waveguide.

The intensity of the light from the output of the AOTF at longer wavelengths than 1100 nm was too low give a signal that was detectable over a length of a few mm. The white light laser should emit up to 2400 nm, and there was an output, but it was less than approximately one hundredth of the signal at the other wavelengths.

Chapter 5

Conclusion and Further Work

This chapter will conclude on the performance of the setup that was built as a part of this thesis and suggest improvements that can be done. The measurements of the losses in the PS waveguide will also be reviewed, and suggestions to possible applications of the setup will be given.

5.1 Experimental Setup

It is shown that it is possible to send light into an AOTF from a different white light source than what the AOTF is built for. The light going into the AOTF has to be polarized, collimated and enter the AOTF straight. A setup that fulfills all these demands has been made, implemented and shown to work. However, there was not enough light going out of the system to do scatter loss measurements on waveguides when using the LDLS as a white light source.

5.2 Loss measurements

The losses in the PS waveguide was found by using a spectrometer and using a detector connected to a lock-in amplifier. The losses were found to vary with wavelength, and the losses did not agree when comparing the two different detection methods, one with the spectrometer and the other with the lock-in amplifier. The losses found by using the spectrometer has high uncertainty associated to it due to the signal-to-noise ratio being low and that the scans had a low resolution. The losses found when using the detector with the lock-in gave

a higher resolution, but mode stripping and excessive scattering from impurities in the film made the losses higher than what they actually are.

Using the LDLS, gave no detectable signal of the light scattered out of the waveguide, neither when using a spectrometer nor when using a lock-in amplifier. There was enough signal for both the spectrometer and the lock-in amplifier when using the white light laser as a source. The lock-in amplifier has a higher signal to signal-to-noise ratio than the spectrometer, making it more desirable to use. The automated scanning process of the lock-in amplifier enables the scans to have a higher resolution, thus giving a more accurate value for the losses.

5.3 Further work

A way to avoid using the white light laser for preliminary experiments is to find a different white light source that is more powerful than the LDLS and which can be collimated without losing much of its intensity. The light source should emit in the same range as the operating range of the AOTF to utilize the full potential of the device. An improvement on the collimation of the white light going into the AOTF may yield a higher throughput of the filter.

Another possibility is to increase the bandwidth of the AOTF to increase the number of photons that will be let through the AOTF. This could be done in combination with a new light source and could possibly yield more light being scattered out of the waveguide. An increase in the bandwidth of the AOTF would deteriorate the validity of wavelength dependent measurements, but it could be sufficient for preliminary measurements. Decreasing the bandwidth of the AOTF again for using it with the white light laser would give measurements with higher precision.

Since the output of the AOTF is only a fraction of the incident light, it is important that as little as possible of the output light is lost. It is possible to have a fiber with a bigger diameter than the Thorlabs GIF625 fiber, which can be drawn at the other end to enable coupling into

the waveguide. One would then eliminate losses associated with coupling between fibers and a fiber with a larger diameter would gather more light, yielding more light being coupled into the waveguide. At the same time, the drawn end of the fiber would have a small enough diameter to yield efficient coupling into the waveguide.

The coupling efficiency of the end-fire coupling is low, with almost 90 % of the light being lost. This is mostly due to the diameter of the fiber used for coupling into the waveguide being a few microns, while the thickness of the waveguide is approximately 400 nm. The amount of the light that is lost can be decreased by having a thicker film, but there is a limit to how thick the film can be while it is still able to waveguide. It is also possible to use a index-matching fluid to decrease the divergence angle of the bare end fiber, thus coupling more of the light into the waveguide.

The setup with the tunable filter has many interesting applications, one of which have been indicated by the results presented in section 4.3.3. The AOTF could allow characterization of the wavelength dependent features of fluorescent impurities. A waveguide containing desired impurities could be made and investigated using the setup with the white light laser, the AOTF and the lock-in detection of the scattered light using the stepper motor to scan the surface of the waveguide. If the material used for making the waveguide has a refractive index that varies more with wavelength than the refractive index of the polystyrene, it might be necessary to move the coupling spot between each wavelength to make sure the same impurity is hit by the guided light. The setup designed is also able to measure losses in waveguides, but the waveguide should have a higher purity with less scattering centers than the PS waveguide reported here.

Appendix A

Detailed Description of the Experimental Setup

This appendix is meant for anyone who is interested in working further on the set up made as a part of this thesis. Here, details will be explained needed for make the system function and aligning the components.

A.1 Input to AOTF

The fiber going from the plasma source to the reflective collimator is a UVFIBERX-455 from Energetiq. This has an FC-connection that is connected to the light source and an SMA-connector at the other end going into the reflective collimator. The reflective collimator (Thorlabs, RC02SMA-F1) is mounted into a SM1A6 adapter from Thorlabs. This adapter makes it possible to attach the reflective collimator to a lens tube. The UV-fitler and the lens (with a focal length equal to 500 mm) is mounted in the same lens tube that is connected to the reflective collimator.

A double Glan Taylor polarizer (Thorlabs, DGL10) is mounted in a separate lens tube and connected to the rotation mount (PRM1, Thorlabs). The lens tube that is holding the reflective collimator and containing the UV-filter and the lens has to be placed so that it is touching the surface of the other side of the rotation mount. This will ensure that the two lens tubes are aligned. The height of the lens tube with the reflective collimator can be changed,

but it should be in a height that gives the highest throughput of the AOTF.

The smallest end of the alignment tool fits into the lens tube containing the polarizer. The polarizer should be mounted in the lens tube in such a way that allow the alignment tool to fit into it as well. The other side of the alignment tool fits on the outside of the input piece of the AOTF. When all the parts are placed together, there is a little wiggle room. The easiest way to check the alignment is to put a detector at the output of the AOTF and change the alignment a little to get the highest throughput.

A.2 Output from AOTF

The AOTF came with two fibers, one for the NIR1 output and one for the NIR2 output. Both fibers also came with two collimators for each end of the fiber. The collimators fits into the output piece of the AOTF and the position of the collimator can be optimized by turning four set screws. This procedure may be time consuming, but it is explained in detail in the manual of the AOTF. The side of the fiber going into the AOTF is labeled "NIR1 intput" and the collimator at the other end of the fiber is labeled "output".

Appendix B

Calculations

Here, the solution of the equation

$$k_a^2 = k_d^2 + k_i^2 - 2k_d k_i \cos(\theta_d + \theta_i). \tag{B.1}$$

will be given in detail.

Rearranging the terms in eq. (B.1) gives

$$\begin{aligned}
\frac{f^2}{v^2} &= \frac{1}{\lambda_0^2}\left[n_d^2 + n_i^2 - 2n_d n_i \cos(\theta_d + \theta_i)\right] \\
\frac{\lambda_0^2}{\Lambda^2} &= n_d^2 + n_i^2 - 2n_d n_i \cos(\theta_d + \theta_i) \\
\frac{\lambda_0^2}{\Lambda^2} &= n_d^2 + n_i^2 - 2n_d n_i (\cos\theta_d \cos\theta_i - \sin\theta_d \sin\theta_i) \\
\cos\theta_d \cos\theta_i - \sin\theta_d \sin\theta_i &= \frac{n_d^2 + n_i^2}{2n_d n_i} - \frac{\lambda_0^2}{2n_d n_i \Lambda^2}.
\end{aligned}$$

It has been used that $\Lambda = {}^{v}/_{f}$ and the relation $\cos(x+y) = \cos x \cos y - \sin x \sin y$.

The relations $a = k_d \sin\theta_d$, $b = k_i \sin\theta_i$, $c = k_i \cos\theta_i$ and $k_a = a + b$ are found from the ge-

ometry of fig. 2.3b. Substituting for $\cos\theta_i$ and $\sin\theta_i$ gives

$$\begin{aligned}
\cos\theta_d \cdot \frac{c}{k_i} - \sin\theta_d \cdot \frac{b}{k_i} &= \frac{n_d^2 + n_i^2}{2n_d n_i} - \frac{\lambda_0^2}{2n_d n_i \Lambda^2} \\
\cos\theta_d \cdot \frac{k_d \cos\theta_d}{k_i} - \sin\theta_d \cdot \frac{k_a - k_d \sin\theta_d}{k_i} &= \frac{n_d^2 + n_i^2}{2n_d n_i} - \frac{\lambda_0^2}{2n_d n_i \Lambda^2} \\
\frac{k_d}{k_i}\cos^2\theta_d - \frac{k_a}{k_i}\sin\theta_d + \frac{k_d}{k_i}\sin^2\theta_d &= \frac{n_d^2 + n_i^2}{2n_d n_i} - \frac{\lambda_0^2}{2n_d n_i \Lambda^2} \\
\frac{k_d}{k_i} - \frac{k_a}{k_i}\sin\theta_d &= \frac{n_d^2 + n_i^2}{2n_d n_i} - \frac{\lambda_0^2}{2n_d n_i \Lambda^2}.
\end{aligned}$$

Using that

$$\frac{k_d}{k_i} = \frac{n_d}{n_i} \text{ and } \frac{k_a}{k_i} = \frac{f\lambda_0}{v n_i}$$

one get

$$\begin{aligned}
\frac{n_d}{n_i} - \frac{f\lambda_0}{v n_i}\sin\theta_d &= \frac{n_d^2 + n_i^2}{2n_d n_i} - \frac{\lambda_0^2}{2n_d n_i \Lambda^2} \\
\sin\theta_d &= \frac{\Lambda n_d}{\lambda_0} - \frac{\Lambda(n_d^2 + n_i^2)}{2n_d n_i} + \frac{\lambda_0}{2n_d \Lambda} \\
\sin\theta_d &= \frac{\Lambda^2(2n_d^2 - n_d^2 - n_i^2) + \lambda_0^2}{2n_d \lambda_0 \Lambda} \\
\sin\theta_d &= \frac{\Lambda(n_d^2 - n_i^2)}{2n_d \lambda_0} + \frac{\lambda_0}{2n_d \Lambda} \\
\sin\theta_d &= \frac{\lambda_0}{2n_d \Lambda}\left[1 - \frac{\Lambda^2}{\lambda_0^2}(n_i^2 - n_d^2)\right].
\end{aligned}$$

Similarly, but now replacing $\cos\theta_d$ and $\sin\theta_d$ instead of $\cos\theta_i$ and $\sin\theta_i$ and solving the equation in the same way, but with respect to $\sin\theta_i$ gives

$$\sin\theta_i = \frac{\lambda_0}{2n_i \Lambda}\left[1 + \frac{\Lambda^2}{\lambda_0^2}(n_i^2 - n_d^2)\right].$$

Bibliography

[1] IC Chang. Acoustooptic devices and applications. *IEEE transactions on sonics and ultrasonics*, 23(1):p2, 1976.

[2] Heidi Hall, Mark Bridges, Silas Leavesley, and J Paul Robinson. Design of a wavelength-tunable light source using an acousto-optic tunable filter. In *Optical Engineering+ Applications*, pages 66680W–66680W. International Society for Optics and Photonics, 2007.

[3] Brimrose. Aotf tunable light sources (tls-300). `http://brimrose.com/pdfandwordfiles/AOTF_LS.pdf`, 22, 6 2017. Accessed: 2017-06-22.

[4] Thomas A Strasser and Mool C Gupta. Optical loss measurement of low-loss thin-film waveguides by photographic analysis. *Applied optics*, 31(12):2041–2046, 1992.

[5] E. V. Andreeva, L. N. Magdich, D. S. Mamedov, AA Ruenkov, M. V. Shramenko, and S. D. Yakubovich. Tunable semiconductor laser with an acousto-optic filter in an external fibre cavity. *Quantum Electronics*, 36(4):324, 2006.

[6] K Takabayashi, K Takada, N Hashimoto, M Doi, S Tomabechi, T Nakazawa, and K Morito. Widely (132 nm) wavelength tunable laser using a semiconductor optical amplifier and an acousto-optic tunable filter. *Electronics Letters*, 40(19):1187–1188, 2004.

[7] Kazumasa Takada and Hiroaki Yamada. Narrow-band light source with acoustooptic tunable filter for optical low-coherence reflectometry. *IEEE Photonics Technology Letters*, 8(5):658–660, 1996.

[8] IC Chang. Acousto-optic tunable filters. *Optical Engineering*, 20(6):206824–206824, 1981.

[9] IC Chang. Tunable acousto-optic filters: an overview. In *20th Annual Technical Symposium*, pages 12–22. International Society for Optics and Photonics, 1976.

[10] IC Chang. Noncollinear acousto-optic filter with large angular aperture. *Applied Physics Letters*, 25(7):370–372, 1974.

[11] Ling Bei, Glenn I Dennis, Heather M Miller, Thomas W Spaine, and Jon W Carnahan. Acousto-optic tunable filters: fundamentals and applications as applied to chemical analysis techniques. *Progress in Quantum Electronics*, 28(2):67–87, 2004.

[12] R Dixon. Acoustic diffraction of light in anisotropic media. *IEEE Journal of Quantum Electronics*, 3(2):85–93, 1967.

[13] Chieu D Tran. Acousto-optic devices: optical elements for spectroscopy. *Analytical chemistry*, 64(20):971A–981A, 1992.

[14] Louis J Denes, Milton S Gottlieb, and Boris Kaminsky. Acousto-optic tunable filters in imaging applications. *Optical Engineering*, 37(4):1262–1267, 1998.

[15] José E. B Oliveira. *Generalized anisotropic acoustooptic diffraction in uniaxial crystals*. PhD thesis, McGill University, Montreal, Canada, 1 1986.

[16] IC Chang and J Xu. High performance aotfs for the ultraviolet. In *Ultrasonics Symposium, 1998. Proceedings., 1998 IEEE*, volume 2, pages 1289–1292. IEEE, 1998.

[17] P Katzka and IC Chang. Noncollinear acousto-optic filter for the ultraviolet. In *23rd Annual Technical Symposium*, pages 26–32. International Society for Optics and Photonics, 1980.

[18] Robert G Hunsperger and Jurgen R Meyer-Arendt. Integrated optics: theory and technology. *Applied Optics*, 31:298, 1992.

[19] Xingcun Colin Tong. *Advanced materials for integrated optical waveguides*, volume 46. Springer, 2014.

[20] Paul DT Huibers and Dinesh O Shah. Multispectral determination of soap film thickness. *Langmuir*, 13(22):5995–5998, 1997.

[21] K Gut and K Nowak. Determination of the attenuation of planar waveguides by means of detecting scattered light. *The European Physical Journal-Special Topics*, 154(1):89–92, 2008.

[22] Eugene Hecht. *Optics*, volume 4. Pearson, 2014.

[23] Yasuyuki Okamura, Shinji Yoshinaka, and Sadahiko Yamamoto. Measuring mode propagation losses of integrated optical waveguides: a simple method. *Applied Optics*, 22(23):3892–3894, 1983.

[24] Thorlabs Inc. Rc02sma-p01 - protected silver reflective collimator. `https://www.thorlabs.com/thorproduct.cfm?partnumber=RC02SMA-P01`, 24, 5 2017. Accessed: 2017-05-24.

[25] David B Hall, Patrick Underhill, and John M Torkelson. Spin coating of thin and ultrathin polymer films. *Polymer Engineering & Science*, 38(12):2039–2045, 1998.

[26] Kyu J Lee, Debra Wawro, Purnomo S Priambodo, and Robert Magnusson. Agarose-gel based guided-mode resonance humidity sensor. *IEEE Sensors Journal*, 7(3):409–414, 2007.

[27] Fianium. Aotf and aotf-dual systems product datasheet. `http://www.fianium.com/pdf/sc_aotf_v2.pdf`, 25, 5 2017. Accessed: 2017-05-25.

[28] N Sultanova, S Kasarova, and I Nikolov. Dispersion proper ties of optical polymers. *Acta Physica Polonica-Series A General Physics*, 116(4):585, 2009.